Structural Origins of Crack Resistance on Magnesium Aluminoborosilicate Glasses Studied by Solid State NMR

Henrik Bradtmüller,[a] Tobias Uesbeck,[a] Hellmut Eckert,[a,b*]

[a]Institut für Physikalische Chemie, Westfälische Wilhelms-Universität Münster, Corrensstraße 30, D-48149 Münster, Germany.

[b]Instituto de Física de São Carlos, Universidade de São Paulo, CP 369, 13566-590, São Carlos, SP, Brasil.

Tetsuya Murata,[c] Shingo Nakane,[c] Hiroki Yamazaki[c]

[c]Nippon Electric Glass, Otsu Japan, 7-1, Seiran 2-chome, Otsu, Shiga 520-8639, Japan.

ABSTRACT

The beneficial effect of magnesium oxide upon the performance of crack resistant oxide glasses has been explored in a series of aluminoborosilicate glasses with the compositions $60SiO_2$-(20-*x*)Al_2O_3-*x*B_2O_3-$20Na_2O$ and $60SiO_2$-(20-*x*)Al_2O_3-*x*B_2O_3-$10Na_2O$-10MgO. The simultaneous presence of both boron and aluminum oxides in these glasses produces a synergetic effect upon the crack resistance, the structural origins of which are being explored by detailed ^{11}B, ^{23}Na, ^{27}Al, and ^{29}Si single and double resonance solid state NMR studies. Aluminum is exclusively four-coordinated, whereas the boron is found in both three- and four-coordination. Substitution of B_2O_3 with Al_2O_3 and Na_2O with MgO leads to a dramatic reduction of N_4, the fraction of four-coordinate boron, accompanied by an increase in crack resistance. $^{11}B/^{27}Al$ double resonance NMR studies show only weak interactions between the boron oxide and aluminum oxide components, giving no evidence of the formation of new structural units not already realized in the (pseudo)-ternary aluminosilicate and borosilicate glass systems. Rather, the effect of magnesium can be related to a dramatic reduction of the fraction of four-coordinate boron species compared to the analogous sodium-based system. This reduction results from a preference of the sodium ions to charge-compensate anionic $AlO_{4/2}^-$ species, combined with an unfavorable interaction of four-coordinate boron with Mg^{2+}. Overall, the results give important insights into the Mg-driven structural network changes in this four-component glass system providing a structural rationale for the dramatic effect of magnesium upon the mechanical properties of these glasses.

INTRODUCTION

Ultrastrong glasses with high crack resistance are of great interest for the optimization of low-weight flat displays in modern handheld electronic devices. In this context intense development efforts are devoted to new oxide glass formulations for improving the mechanical strengths without compromising other physical properties.[1-8] An important issue in this regard has been the conflicting demand of hardness and crack resistance upon the glass composition. While high packing densities promote hardness, they tend to limit the ability of deflecting mechanical stresses, i.e. they tend to lower crack resistances, as shown for various silicate,[2] borosilicate,[3,4] aluminosilicate,[5] and aluminoborate glass compositions.[6] Recently, glass compositions including high-field strength cations have shown promise of overcoming this dilemma. For example, within the Al_2O_3-SiO_2 glass system the hardness and crack-resistance increase simultaneously with increasing Al_2O_3 content, an effect that can be linked to Al^{3+} ions, occurring in five- and six-fold coordination.[7] Another example is found in the series of alkaline-earth aluminoborate glasses where hardness and crack resistance increase concomitantly along the series Ba->Sr->Ca->Mg.[8] Based on the latter result the incorporation of magnesium into borosilicate, aluminosilicate, and aluminoborosilicate glasses appears very promising. To guide further research in this direction it will be important to develop a fundamental understanding of the structural origins of crack resistance. Being one of the most powerful structural characterization techniques, nuclear magnetic resonance has already provided some important insights into this matter.[4-6,8] Crack resistance may be correlated with various structural features related to the short-range order environment of the boron and aluminum species. In borosilicate glasses, crack resistance was shown to decrease with increasing fraction of four-coordinated boron atoms.[4] In aluminosilicate and aluminoborate glasses, crack resistance was shown to increase with increasing average coordination number (presence of higher-coordinated aluminum species).[5,7] In the alkaline-earth aluminoborate glasses of reference[8] exactly these structural changes are observed, accompanied by a dramatic increase in crack resistance, when sodium oxide is substituted by magnesium oxide at constant network former composition (constant total modifier content). Similar benefits might be expected, if both structural modification mechanisms could be combined within glass formulations that are based on silicate glasses containing magnesium oxide together with both aluminum and boron oxide network former species. This potential synergy will be explored in the present contribution, by conducting a systematic study of the structure-property relation in magnesium-containing aluminoborosilicate glasses. Here we report the preparation and mechanical characterization of glasses in the tectosilicate analogue systems $60SiO_2$-$(20-x)Al_2O_3$-xB_2O_3-$20Na_2O$ and $60SiO_2$-$(20-x)Al_2O_3$-xB_2O_3-$10Na_2O$-$10MgO$. The physical property measurements are correlated with systematic structural studies combining results from ^{11}B, ^{23}Na, ^{27}Al, and ^{29}Si single and double resonance solid state NMR studies. While a large number of

multinuclear NMR results on alkali- and alkaline earth aluminosilicate and aluminoborosilicate glasses can be found in the literature,[9-28] the structural evolution along the present compositional section has not been studied previously. Also, more advanced NMR techniques have been rarely applied to these compositionally rather complex glasses. The results of the present study, interpreted within the relevant literature context, give insights into the Mg-driven structural network changes in this four-component system, providing a structural rationale for the dramatic effect of magnesium upon the mechanical properties of these glasses.

EXPERIMENTAL

Sample preparation and Characterization. Table 1 summarizes the glass compositions and the physical properties measured. The batches were mixed thoroughly and melted in 500 cm^3 Pt crucibles at 1100 to 1650°C for about 22 h in an electric furnace. The melting temperature for each composition was chosen according to the viscosity of the melt. After the melting period the glass melts were poured onto a carbon plate, and then placed in an electric furnace to cool slowly. Glass transition temperatures, T_g, were determined by a dilatometer. The cooled glass was heated up to the temperature of (T_g + 30°C), held for 30 min, and then cooled by 3°C/min to obtain annealed glasses. Samples of the glasses were ground, lapped with Al_2O_3 slurry, and then finished with cerium oxide to get optically smooth surfaces, which were used for the following indentation tests.[4] Further physical properties measured include density (ρ) and Young's modulus (E). Density was measured by Archimedes's method. Young's modulus was determined by a resonance method. The crack resistance value (CR) was measured by Vickers indentation tests.[29,30] The glass sample was exposed to a Vickers diamond indenter in air (25°C, 30% relative humidity), for a loading time of 15 s, and the corners where radial cracks appeared were counted with an optical microscope 15 s after unloading. When a glass sample is indented, various types of cracks form around the indenter. Only radial cracks are counted for determining crack resistance, because the cracks normal to the glass surface are critical to glass fracturing. The percentage of crack initiation was determined as the ratio of the number of the corners with the cracks to the total number of the corners of indentations. The applied load was stepwise increased and twenty indentations were made for each applied load. The load at which the percentage equals 50% is determined as "crack resistance", CR.

Table 1: Compositions (in mole %) and physical properties of the glasses measured.

SiO_2	B_2O_3	Al_2O_3	Na_2O	MgO	*CR*(gf)	T_g(°C)	ρ(g/cm^3)	*V*(cm^3)	*E*(GPa)
60	20	0	20	0	30	566	2.52	24.76	82
60	20	0	10	10	700	556	2.40	25.09	73
60	15	5	20	0	700	570	2.48	25.81	76
60	15	5	10	10	1800	572	2.39	25.87	70
60	10	10	20	0	1000	562	2.46	26.67	73
60	10	10	10	10	1700	604	2.40	26.44	69
60	5	15	20	0	800	574	2.45	27.44	70
60	5	15	10	10	2000	671	2.44	26.62	76
60	0	20	20	0	300	788	2.46	28.00	68
60	0	20	10	10	750	747	2.51	26.75	84
60	0	20	0	20	2200	819	2.59	24.91	101

Solid State NMR. Single resonance MAS NMR spectra were recorded at 5.7, 9.4, 11.7, and 14.1 T using an Agilent DD2 spectrometer, Bruker DSX-500 and -400 spectrometers and a Bruker Avance Neo 600 MHz spectrometer. Single-pulse ^{11}B, ^{23}Na, ^{27}Al and ^{29}Si high-resolution solid-state NMR spectra were measured with commercial MAS-NMR probes operated under the conditions specified in Table 2. Chemical shifts are reported relative to aqueous solutions of 0.1 M NaCl, 1 M $Al(NO_3)_3$, TMS, and BF_3-Et_2O solution and solid secondary standards of NaCl, AlF_3, tetrakis-trimethyl silyl silane and BPO_4. ^{11}B MAS-NMR spectra were fitted with the DMfit program,[31] assuming second-order perturbation theory for the simulation of the three-coordinated boron species whereas the signals or the four-coordinated boron were approximated by Gauss-Lorentz curves. No intensity correction was done for satellite transition MAS sideband intensity contributing to the central ^{11}B MAS-NMR line of the $B^{(4)}$ units. The ^{23}Na and ^{27}Al MAS-central transition spectra were fitted according to the Czjzek model,[32] implemented within the DMfit data processing and simulation program.[31] Consistent fitting parameters were obtained for the ^{27}Al MAS-NMR spectra measured for all the samples at 5.7 and 14.1 T (see Supporting Materials Section).

Static ^{23}Na spin echo decay spectroscopy was carried out at 11.7 T employing the standard Hahn echo pulse sequence with selective excitation pulses of about 12.5 µs length corresponding to a nutation frequency of 10 kHz.[33] The Hahn Echo intensities were recorded for a range of interpulse delays up to $2\tau_1$ = 1000 µs, while τ_1 was incremented in smaller steps in the initial time regime. The experiments were performed at 190 K to eliminate any ^{23}Na ionic motion that could produce

contributions to the echo decay from dynamic relaxation which would tend to overestimate second moment values.

^{23}Na and Triple Quantum Magic Angle Spinning (TQMAS) spectra were recorded at carrier frequencies of the MAS NMR experiments using a z-filtered three-pulse sequence.[34] The employed pulse lengths were close to 6.25 and 2.0 μs at a nutation frequency of 100 kHz for the first two hard pulses. The duration of the soft third pulse was 10.0 μs at a nutation frequency of 12.5 kHz. All the samples were spun at the magic angle with a frequency of 14.0 kHz. ^{27}Al triple-quantum (TQ)-MAS-NMR spectra were measured at 14.1 (and 11.7) T at a spinning speed of 15.0 (12.5) kHz using the same sequence. At a ^{27}Al nutation frequency of 130 kHz (90 kHz) the hard excitation and reconversion pulses were 2.75 (4.0 to 4.5) and 1.0 (1.2-1.5) μs long. The third soft detection pulse had a length of 10 μs at a nutation frequency of 10 kHz. The relaxation delay was 1s. For all the TQMAS experiments, acquisition of the indirect dimension was synchronized with the rotors' spinning speed and for sampling in the t_1 dimension dwell times of 8.93 μs and 33 μs (20 μs) were chosen for ^{23}Na and ^{27}Al respectively. The data is shown after shearing transformation with sum projections of the high and low-resolution spectra along the $F1$ and $F2$ axis respectively. For values of the second order quadrupole effect (*SOQE*) and the isotropic chemical shift (δ_{CS}^{iso}) the signal's centers of gravity in $F1$ and $F2$ dimensions were evaluated.

The specific methodology used for the double resonance experiments is described in the Supporting Materials Section, and the pulse sequences used are displayed in Figure S1. Both Rotational Echo DOuble Resonance (REDOR)[35] and Rotational Echo Adiabatic Passage DOuble Resonance (REAPDOR)[36] experiments were employed. ^{11}B{^{27}Al} REDOR experiments were done at 14.1 T, at a spinning frequency of 15.0 kHz, using 180° π pulses of 2.7 – 3.2 μs length on the ^{27}Al recoupling channel at a nutation frequency of 130 kHz. ^{11}B{^{23}Na} REDOR experiments were carried out on a Bruker DSX 500 MHz spectrometer using a 4 mm Bruker triple resonance probe at a MAS spinning frequency of 15.0 kHz and ^{23}Na 180° π pulse durations of about 16.0 μs length. All ^{11}B observed REDOR experiments were performed twice for each glass composition with the optimized 90° and 180° pulse lengths of the three and four coordinated boron species respectively. The π-pulses applied at the re-coupling channel were phase cycled according to the XY-4 scheme.[37] Single-point ^{29}Si{^{27}Al} REAPDOR experiments were conducted at 11.7 T, at 10.0 kHz spinning frequency, using a rotor synchronized Hahn spin echo sequence (π pulse length 21.4

- 23.4 µs) for ^{29}Si detection. Dipolar recoupling was done by ^{27}Al continuous-wave irradiation at a nutation frequency of 20 kHz (liquid sample) for 1/3 of the rotor period.

Table 2: Zeeman frequencies ν_0, 90° pulse lengths t_{90}, relaxation delays $D1$, MAS spinning speeds ν_r and number of scans *NS* applied in the MAS NMR experiments.

Nucleus	ν_0 / MHz	t_{90} / µs	$D1$ / s	ν_r / kHz	*NS*
^{11}B	77.8	1.0	10	14.0	1600
^{23}Na	132.3	1.0	0.5	15.0	4096
^{27}Al	156.4	1.0	0.3	15.0	40000
^{29}Si	48.2	6.3	1800	5.0	48

RESULTS, DATA ANALYSIS, AND INTERPRETATION

Composition dependent bulk properties. Table 1 summarizes the bulk physical properties measured. For all of the glasses containing 20 mole % Na_2O as the network modifier component, the molar volumes increase with increasing Al content, while the E-modulus shows a monotonic decrease. These results suggest a continuous decrease in packing efficiency. For the glasses containing 10 mole% Na_2O and 10 mole% MgO, the increase of molar volume with increasing Al content is much less pronounced and the E-modulus passes through a minimum at x = 10, suggesting two mutually compensating effects of composition. Glasses at the high-boron end behave similarly as the pure sodium-containing glasses whereas in glasses at the high-aluminum end (x = 5 and 0) the opposite trend is observed: substitution of Na_2O by MgO produces a decrease in molar volume, an increase in the E-modulus and an increase in the glass transition temperature. These results highlight again the special effect of magnesium oxide upon the physical properties of aluminosilicate glasses, which is quite different from the situation in borosilicate glasses.

Regarding crack resistance, the following observations are made:

1) Partial replacement of Na by Mg leads to dramatic enhancement in crack resistance at any basic network composition. The endmember glass $20MgO\text{-}20Al_2O_3\text{-}60SiO_2$, in which all of the Na_2O can be substituted by MgO shows the highest *CR* value.

2) In the boroaluminosilicate glasses and the borosilicate endmember glass, only half of the Na_2O can be replaced by MgO without the occurrence of crystallization. The *CR* values of the

mixed network former glasses are significantly higher than those observed in the compositionally analogous sodium/magnesium aluminosilicate or borosilicate endmember glasses (all having the same MgO content of 10 mole%). This *network former mixing effect* is also noted, albeit to a lesser extent, for the pure sodium boroaluminosilicate glasses. Thus, there seems to be a particular synergetic effect of the simultaneous presence of boron and aluminum in these glasses. One of the goals of the present study is to elucidate the structural origin of it. To assess the relative importance of the boron and the aluminum contents and their speciations in controlling the crack resistance values and to assess the influence of the magnesium upon their speciations in glasses containing both boron and aluminium, a comprehensive NMR study was undertaken, producing (1) information on the network former speciations drawn from ^{29}Si, ^{11}B, and ^{27}Al MAS-NMR spectra, and (2) information concerning medium-range order based on ^{23}Na-^{23}Na, ^{27}Al-^{11}B and ^{23}Na-^{11}B high resolution dipolar spectroscopies. In addition, the local environments of the sodium ions were characterized by high-resolution ^{23}Na MAS-NMR.

^{27}Al MAS-NMR: Figure 1 shows the ^{27}Al MAS-NMR spectra of the series of pure sodium magnesium aluminosilicate glasses. Only the central m = ½ <-> m = -½ Zeeman transition of the ^{27}Al nuclear spins (I = 5/2) is observed. The spectrum of the purely Na-containing glass shows the typical asymmetric lineshape centered around 55 ppm (isotropic chemical shift 62±1 ppm), suggesting that most Al is four-coordinate. However, in order to successfully simulate the lineshape with Czjzek's model of randomly distributed quadrupolar parameters[31] a minor second component (4%) is required to account for signal intensity at the low frequency end of the spectrum. This second component's isotropic shift of 33 ppm indicates the presence of some Al$^{(5)}$ which agrees with findings of Al$^{(5)}$ species in the mixed Na-Mg and pure Mg glasses, discussed further below, which show identical chemical shifts and quadrupolar lineshape parameters. Overall, this result stands in good agreement with the findings in the literature on charged balanced sodium aluminosilicate glasses:[28,38,39] For the chosen compositions, all the anionic $AlO_{4/2}^-$ sites can be charge balanced by sodium ions, producing a nearly fully polymerized tetrahedral network as known, for example, in the case of the silica-nepheline diagram,[40] which also includes the composition of the present glass system.

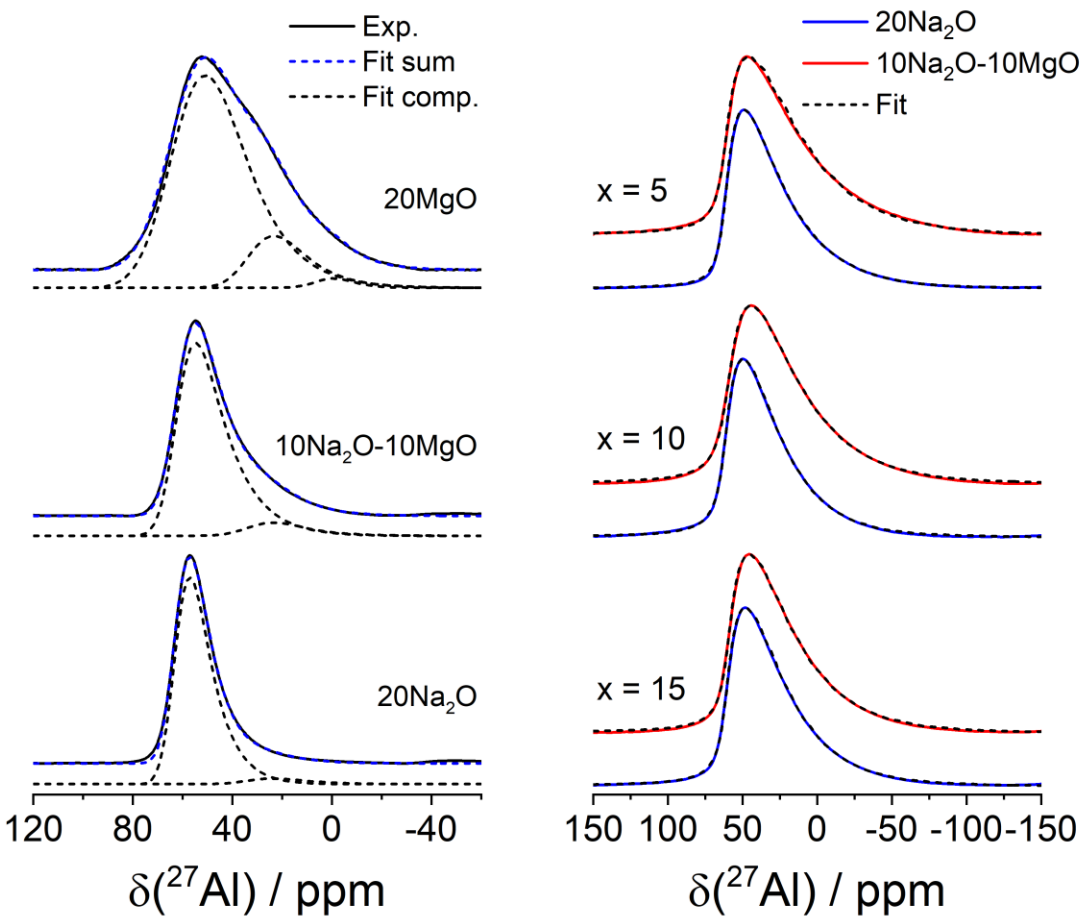

Figure 1: *Left*: ^{27}Al MAS-NMR spectra at 11.7 T of aluminosilicate glasses with compositions $60SiO_2$-$20Al_2O_3$-$20M_{(2)}O$ and varying Na_2O/MgO network modifier composition. *Right*: ^{27}Al MAS-NMR spectra at 5.7 T of the glasses $60SiO_2$-$(20\text{-}x)Al_2O_3$-xB_2O_3 with $20Na_2O$ and $10Na_2O$-10MgO as network modifier. Dashed curves are simulations based on the Czjzek model.

The ^{27}Al MAS-NMR lineshapes of the two Mg-containing glasses, however, appear distinctly different. While they also suggest the majority of the Al species to be four-coordinated, the systematic broadening of the spectrum towards lower frequencies raises the question whether there may be hidden contributions from five- and six-coordinated aluminum. A similar situation is seen for the aluminoborosilicate glasses of the present series (see Figure 1 (right)). Here the effect appears not quite as strong owing to the fact that only 50% of the sodium oxide was replaced by magnesium oxide without inducing crystallization. The systematic difference between the pure Na- and the Na-Mg boroaluminosilicate glasses is seen both at 5.7 and 14.1 T (see Figure S2, Supporting Materials Section); in Figure 1b the spectra obtained at the lower field are shown because the difference appears more accentuated here. Overall the broadening effect caused by MgO substitution seems to decrease as Al_2O_3 is being successively substituted by B_2O_3.

To probe for the possible occurrence of five- and six-coordinated Al in these samples, we conducted (a) ^{27}Al satellite transition (SATRAS)[22,41,42] and (b) ^{27}Al triple quantum MAS-NMR studies. Both experiments enhance the spectroscopic resolution by minimizing anisotropic broadening of the ^{27}Al MAS-NMR spectra due to second-order quadrupolar effects. A small amount of higher-coordinate aluminum is visible in both the TQMAS- and the SATRAS data for the Na_2O-free sample $60SiO_2$-$20Al_2O_3$-20MgO, as indicated in Figure S3 (Supporting Materials Section). In that sample, the amount of higher-coordinated aluminum is estimated to 16±2% $Al^{(5)}$ and 2±2% $Al^{(6)}$. These values are found in excellent agreement with previous studies of this glass composition[25] or compositionally closely related magnesium aluminosilicate glasses.[26,27] The concentration of $Al^{(5)}$ in these aluminosilicate glasses decreases sharply when Mg is successively being replaced by Na.

In contrast to the situation in $60SiO_2$-$20Al_2O_3$-20MgO and $60SiO_2$-$20Al_2O_3$-$10MgO$-$10Na_2O$ glasses, Figure 1 shows no evidence for higher coordinated Al in the mixed boroaluminosilicate glasses of the present study. This is further confirmed by the SATRAS or the TQMAS-NMR data shown in Figure S4 (Supporting Materials Section). Here, the replacement of Na by Mg does not produce higher-coordinated Al species in significant amounts. The analysis of the TQMAS spectra reveals further that the average ^{27}Al chemical shifts of the mixed modifier glasses (Na/Mg) appear consistently at a lower frequency than the compositionally analogous single modifier (Na) glasses. In agreement with the SATRAS results, significant differences are also observed in the nuclear electric quadrupolar coupling strength (the *SOQE* parameter) listed in Table 3, indicating that the four-coordinated Al species in the mixed Na/Mg glasses experience a stronger electric field gradient than those in the single Na-glasses. This result suggests that charge neutralization of the anionic $Al^{(4)}$ species by Mg^{2+} produces a larger degree of local distortion at the aluminum sites than charge neutralization by Na^+. Two mechanisms promoted by the high-field strength cation Mg^{2+} can be envisioned leading to the formation of Al species not observed in alkali aluminosilicate glasses: Al species involved in either $Al^{(4)}$-O-$Al^{(4)}$ linkages or four-coordinate Al species carrying non-bridging oxygen atoms ($Al^{(3)}$ units). Both would lead to an accumulation of two negative charges in close proximity, which may be compensated by Mg^{2+}.

Table 3: Area fractions, isotropic chemical shifts (± 1.0 ppm), average quadrupole coupling constants C_Q (±0.5 MHz) from MAS lineshape simulations at 5.7 T with the Czjzek model. Independenty determined values of second order quadrupole effect (*SOQE*) (±0.5 MHz) and isotropic chemical shifts extracted from ^{27}Al TQMAS-NMR spectra measured at 14.1 T are also included. $SOQE = C_Q \times (1 + \eta^2/3)^{1/2}$, where C_Q is the quadrupole coupling constant (a measure of the maximal component of the electric field gradient tensor) and η is the electric field gradient asymmetry parameter.

Sample	δ_{iso} / ppm		Avg. C_Q / MHz	*SOQE* / MHz	Area fraction / %
20Na_2O	Czjzek (MAS)	TQMAS	Czjzek (MAS)	TQMAS	Czjzek (MAS)
x = 0 / $Al^{(4)}$	63.3	-	4.9	-	96
x = 0 / $Al^{(5)}$	33.0	-	5.8	-	4
x = 5 / $Al^{(6)}$	62.3	62.1	4.3	4.5	100
x = 10 / $Al^{(4)}$	61.8	61.3	4.2	4.5	100
x = 15 / $Al^{(4)}$	61.4	60.2	4.1	4.5	100
10Na_2O-10MgO					
x = 0 / $Al^{(4)}$	63.0	-	5.8	-	93
x = 0 / $Al^{(5)}$	33.0	-	5.8	-	7
x = 5 / $Al^{(4)}$	62.5	60.3	4.7	5.8	100
x = 10 / $Al^{(4)}$	60.6	59.5	4.5	5.4	100
x = 15 / $Al^{(4)}$	60.2	58.5	4.3	5.2	100
20MgO					
x = 0 / $Al^{(4)}$	63.0	-	6.4	-	82
x = 0 / $Al^{(5)}$	33.0	-	5.9	-	16
x = 0 / $Al^{(6)}$	4.73	-	4.0	-	2

^{11}B MAS-NMR. Figure 2 (left) shows the effect of substitution of Na_2O for MgO upon the ^{11}B MAS-NMR spectra of the three borosilicate glasses in the system 60SiO_2-20B_2O_3-(20-*x*)Na_2O-*x*MgO. The spectra can be deconvoluted into two distinct types of lineshape components, belonging to four-coordinated boron (sharp Gaussian line near 0 ppm, vs BF_3-Et_2O) and two broad two-peaked powder patterns arising from interactions of the ^{11}B nuclear electric quadrupole moment with the strong electrostatic field gradients created by the trigonal planar bonding geometry of three-coordinate boron species. This interaction can again be modeled by second-order perturbation theory with respect to the effect upon the ^{11}B Zeeman levels, resulting in the

characteristic lineshape for the central m = ½ <-> m = -½ transition of the spin-3/2 ^{11}B nuclear isotopes.[42] By quantitative deconvolution of the lineshapes the fractional areas of the three-coordinate boron species could be determined. Table 4 summarizes all the lineshape parameters used for fitting the spectra. Consistent N_4 values and lineshape parameters were obtained for measurements done at 5.7 and 11.7 T. For the pure sodium borosilicate glass, a high fraction of four-coordinate boron, N_4 = 0.73, is measured, consistent with the expected values known from the literature.[43,44] For the three-coordinated boron species the low value of the electric field gradient asymmetry parameter η (0.25±0.03) indicates a close to axially symmetric species such as that known for neutral trigonally coordinated boron, $BO_{3/2}$ ($B^{(3)}$) units. Anionic three-coordinate meta- or pyroborate groups ($B^{(2)}$ or $B^{(1)}$), for which asymmetry parameters near 0.5-0.6 are expected,[45] do not seem to make a major contribution, although minor levels cannot be ruled out. In fact, in the glass with composition $20Na_2O$-$20B_2O_3$-$60SiO_2$, charge balance dictates that minor amounts of non-bridging oxygen species, bonded either to three-coordinate boron or to $Si^{(3)}$ units, must be present. Furthermore, closer inspection of the lineshapes recorded at 11.7 T indicates that there are actually two distinct types of close to axially symmetric $B^{(3)}$ species in the MAS-NMR spectra, showing distinctly different chemical shifts. In prior work from our laboratory, the dominant species near 17 ppm can be identified with $B^{(3)}$ groups essentially only showing connectivity with other boron species whereas the signals located at an isotropic chemical shift near 12 ppm indicate $B^{(3)}$ units taking part in B-O-Si linkages.[46] As documented in Table 4, the former species prevails in our glasses, although Figure 3, left, suggests that the fraction of Si-bonded $B^{(3)}$ units tends to increase with increasing Mg contribution to the cation inventory. At 5.7 T these two species cannot be separately resolved, and only one three-coordinate component has been assumed to fit the data. Again, the low asymmetry parameter of this species is rather clear from these low-field spectra, suggesting that they are majoritorily neutral $B^{(3)}$ species. Finally, Figure 2 (left), reveals a clear compositional effect of Mg substitution: the fraction of four-coordinate boron species is substantially diminished, and quantitatively consistent with the assumption that MgO does not promote $B^{(4)}$ formation at all in these glasses. In the present borosilicate system, the fraction of four-coordinated boron atoms is close to that predicted by the Dell and Bray model,[44] counting exclusively the Na_2O component as the network modifier.

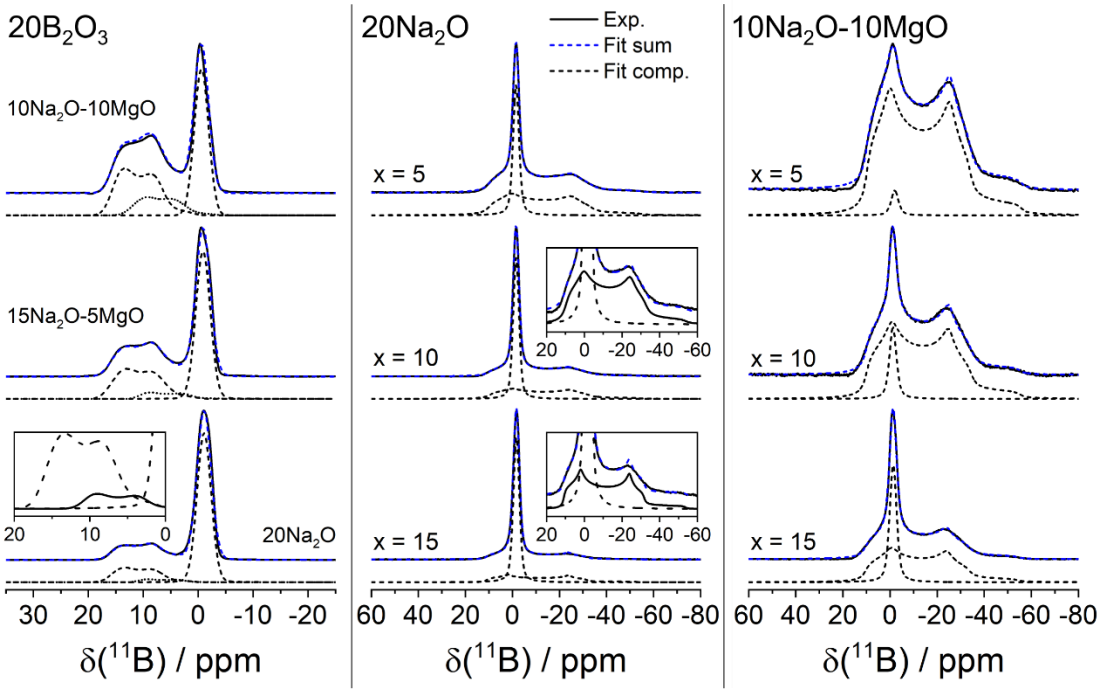

Figure 2: *Left*: ^{11}B-MAS-NMR spectra at 11.7 T of borosilicate glasses in the system with network former compositions $60SiO_2$-$20B_2O_3$ and varying network modifier composition. *Center*: ^{11}B MAS NMR spectra of glasses at 5.7 T with the compositions $60SiO_2$-$(20-x)Al_2O_3$-xB_2O_3-$20Na_2O$. *Right*: ^{11}B MAS NMR spectra at 5.7 T of glasses with the compositions $60SiO_2$-$(20-x)Al_2O_3$-xB_2O_3-$10Na_2O$-10MgO. Dashed curves are simulations done with the DMfit program.

Figure 2 (center and right) shows the ^{11}B MAS-NMR spectra of the six mixed aluminoborosilicate glasses under study. The high fractions of four-coordinate boron (N_4-values) measured in the Mg-free sodium borosilicate glasses suggest the formation of $B^{(4)}$-O-Si linkages that stabilize the four-coordinated boron atoms beyond the limit usually reached (42-50%) in pure alkali borate glasses. This effect is well-documented in the NMR literature,[43] and has been described quantitatively by the model of Dell and Bray.[44] For the boroaluminosilicate glasses, N_4 decreases with increasing Al content, reflecting the preferential association of $Al^{(4)}$ units with the Na^+ cations, reducing their amount available for the stabilization of $B^{(4)}$ units.[16-20,23] Furthermore, as already described above for the sodium magnesium borosilicate glasses, substitution of Na for Mg leads to a dramatic reduction in N_4 values. Again the small values of η detected for these three-coordinate boron atoms indicate that the $B^{(3)}$ species are dominantly neutral $BO_{3/2}$ units rather than anionic three-coordinate $B^{(2)}$ or $B^{(1)}$ species carrying non-bridging oxygen atoms. The $B^{(3)}$ units formed in these glasses are presumably linked to other borate, aluminate and/or silicate groups. This finding is consistent with the ^{29}Si chemical shift trend, indicating a diminution of $Si^{(4)}$-O-$B^{(4)}$ linkages upon Na → Mg substitution (see below). As argued further in the Discussion and Conclusions Section, the

compositional dependence of N_4 can be interpreted by assuming that MgO does not produce any four-coordinate boron species at all, while Na_2O can do so only to the extent that it is not already consumed by the competing prevalent process leading to formation of $AlO_{4/2}^-$ units, e.g. $Al^{(4)}$ species linked to four bridging oxygen atoms.

Table 4: Fitting parameters of ^{11}B MAS-NMR spectra of glasses measured at 5.7 T (or 11.7 T, *) in the system $60SiO_2$-$(20-x)Al_2O_3$-xB_2O_3-$20Na_2O$ and $60SiO_2$-$(20-x)Al_2O_3$-xB_2O_3-$10Na_2O$-10MgO.

Sample	$B^{(3)}$				$B^{(4)}$		
	I (%) (±1)	δ_{iso} / ppm (±0.5)	C_Q /MHz (±0.1)	η (±0.1)	I (%) (±1)	δ_{iso} / ppm (±0.5)	$FWHM$ / ppm (±0.1)
$20Na_2O$							
x = 5	63	15.8	2.6	0.24	37.0	-1.5	3.0
x = 10	42.5	15.4	2.6	0.24	57.5	-1.6	3.0
x = 15	30	16.9	2.6	0.22	70.0	-1.7	3.0
x = 20	22.0*	17.5* 12.3*	2.6* 2.6*	0.30* 0.17*	72.8*	-1.1*	3.0*
$15Na_2O$-5MgO							
x = 20	35.5*	17.5*	2.6*	0.30*	54.9*	-0.9*	3.1*
	9.6*	12.3*	2.6*	0.17*			
$10Na_2O$-10MgO							
x = 5	97.4	15.6	2.6	0.24	2.6	-2.0	3.7
x = 10	89.5	15.3	2.6	0.27	10.5	-1.2	3.5
x = 15	70.4	15.5	2.6	0.28	29.6	-1.3	3.5
x = 20	40.0*	17.2*	2.6*	0.22*	43.0*	-0.6*	3.1*
	17.0*	13.5*	2.6*	0.31*			

*analysis based on spectra measured at 11.7 T

^{29}Si MAS-NMR and ^{29}Si{^{27}Al} REAPDOR NMR: Figure 3 shows the ^{29}Si MAS-NMR spectra of the sodium magnesium aluminosilicate (a) and the sodium magnesium borosilicate (b) glass systems. No peak resolution into distinct silicon species can be observed. Rather, the spectra show one broad unresolved resonance line, from which the average isotropic chemical shift can be extracted from the center of gravity (see Table 5).

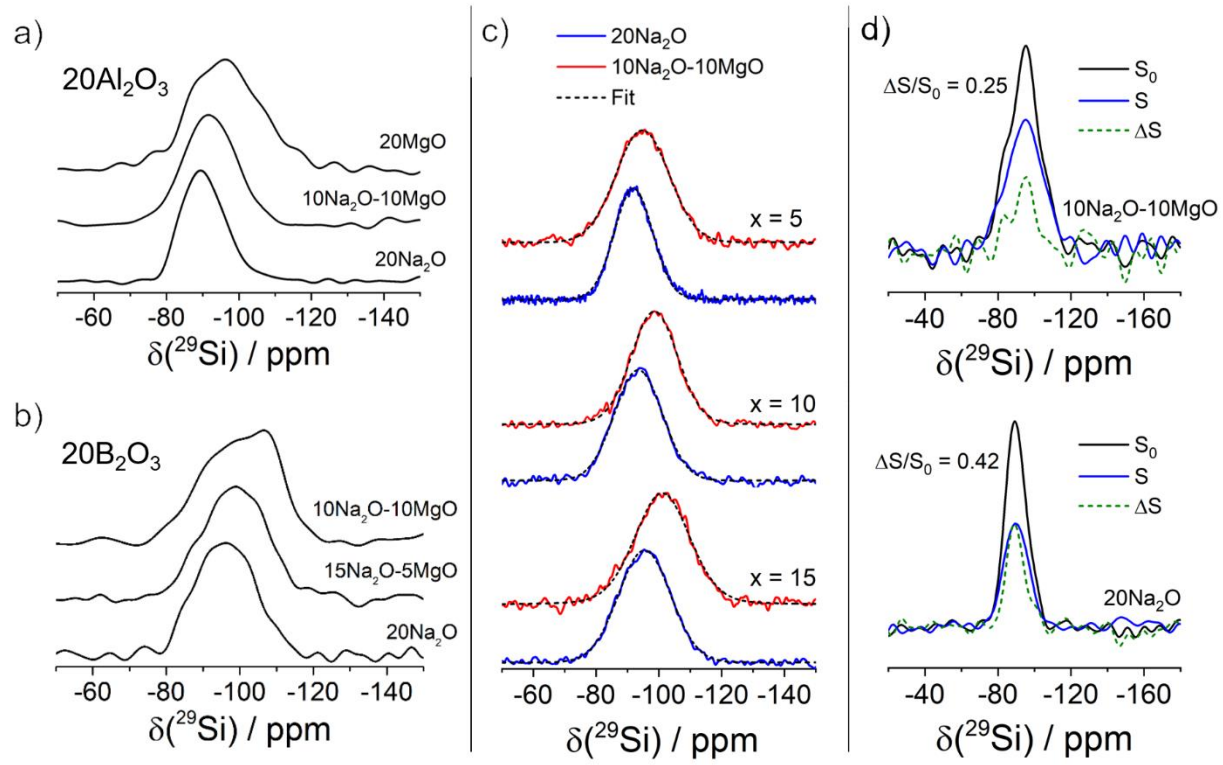

Figure 3: ^{29}Si MAS NMR spectra of sodium magnesium aluminoborosilicate glasses; a) successive replacement of MgO by Na_2O in aluminosilicate glasses, measured at 9.4 T b) successive replacement of MgO by Na_2O in borosilicate glasses, measured at 9.4 T; c): successive replacement of Al_2O_3 by B_2O_3 in the system $60SiO_2$-(20-*x*)Al_2O_3-*x*B_2O_3 with network modifier compositions $20Na_2O$ and $10Na_2O$-10MgO, measured at 5.7 T. Dotted curves indicate Gaussian fits to the data. *d)*: Single point ^{29}Si{^{27}Al} REAPDOR experiments on pure aluminosilicate glasses with $20Na_2O$ (bottom) and $10Na_2O$-10MgO (top). Shown are the echo signal S_0, the diminished REAPDOR echo signal *S* and the difference spectrum $\Delta S = S_0$-*S* for a dipolar mixing time of 2.2 ms. The stronger dipolar recoupling effect in the single modifier glass is evidence for stronger Si-O-Al connectivity.

The spectra suggest the presence of fully polymerized silicon units ($Si^{(4)}$ species), whose resonances are shifted towards higher frequencies compared to the situation in SiO_2, primarily owing to the presence of Si-O-$Al^{(4)}$ and Si-O-$B^{(4)}$ linkages. The shift effect caused by network former mixing is stronger in the aluminosilicates than in the borosilicates. This is consistent with literature data, which indicate that a $Al^{(4)}$-O-Si linkage produces a larger change in ^{29}Si chemical shift than a $B^{(4)}$-O-Si linkage.[23,47] Partial substitution of Na by Mg produces substantial displacements towards lower frequencies by up to 5 ppm. This effect is consistent with a reduction of the average number of Si-O-$X^{(4)}$ (X = B, Al) linkages upon Na → Mg substitution. In the case of the aluminosilicate glasses, the lower extent of Si-O-Al connectivity was further investigated by ^{29}Si{^{27}Al} REAPDOR experiments. These experiments were conducted on a separate set of samples doped with 0.1 mol% MnO, but prepared under otherwise identical conditions. The solid state NMR spectra of these doped samples were measured and found to be identical to those of the

undoped samples (see Figure S3c (right), Supporting Materials Section). Doping was necessary to shorten the ^{29}Si spin-lattice relaxation times in order to acquire spectra within a realistic amount of time. Figure 3d shows the results of single-point REAPDOR acquisitions at a dipolar mixing time of 2200 µs. While in the sodium aluminosilicate glass the dipolar recoupled signal intensity diminished by 42±5%, the attenuation observed for the sodium magnesium aluminosilicate glass was only 25±5%. This important difference shows that substitution of Na_2O by MgO decreases Si-O-Al connectivity in aluminosilicate glasses. Again, this result can be accounted for by the presence of either $Al^{(4)}$-O-$Al^{(4)}$ linkages or $Al^{(3)}$ units (four-coordinate Al attached to one non-bridging oxygen) in the Mg-containing glasses. While in alkali aluminosilicate glasses such units are suppressed because of the unfavorable Coulombic repulsion of two negative charges in close proximity they might be stabilized by high-field strength doubly charged cations such as Mg^{2+}.[13] Similar ^{29}Si chemical shift displacement effects are seen in the mixed Na-Mg-borosilicate glasses, indicating that they have a smaller fraction of $Si^{(4)}$-O-$B^{(4)}$ linkages than the pure Na_2O-based glasses. This is plausible as the fraction of four-coordinate boron is consistently lower in the mixed cation glasses than in the single modifier (Na_2O-) glasses. It was previously shown that while the signals of $Si^{(4)}$ units are shifted to higher frequencies if they are bonded to $B^{(4)}$ groups this is not the case for $Si^{(4)}$-O-$B^{(3)}$ linkages.[47] As discussed above, the latter are identified by ^{11}B MAS-NMR, via a second $B^{(3)}$ signal contribution at a lower isotropic chemical shift.[19,46] The majority of the $B^{(3)}$ units are mostly connected among themselves or with the $B^{(4)}$ species. Thus, the average ^{29}Si chemical shift displacements seen upon Na → Mg substitution are again attributed to an increased proportion of Si-O-Si linkages.

Figure 3b compares the ^{29}Si MAS-NMR spectra of the Na-aluminoborosilicate glasses with those of Na-Mg aluminoborosilicate glasses. Again, the same chemical shift trend is observed, indicating a consistent low-frequency displacement of the center of gravity as half of the sodium oxide is replaced by magnesium oxide. As illustrated by Figure 4 (right) this trend tends to become more pronounced with increasing B_2O_3 contribution to the group 13 metal oxide inventory. At the same time, compared to the glasses containing only sodium as the cationic species, the ^{29}Si MAS-NMR spectra of the Mg-containing glasses are significantly broader, suggesting a wider spread of $Si^{(n)}_{mAl/B}$ units. In particular, the formation of $Si^{(3)}$ species, frequently postulated to be promoted by the high-field strength cations such as Ca^{2+} and Mg^{2+}, cannot be ruled out by these data. [7,8,11-15] Such units would give rise to signals near or below -90 ppm, where indeed substantial signal

intensity is observed as a shoulder in the Mg containing glasses. Owing to the poor resolution and the limited signal-to-noise ratio of these spectra, unambiguous deconvolutions of the ^{29}Si MAS-NMR spectra are not possible here. To resolve the possible occurrence of $Si^{(3)}$ species and their enhanced formation promoted by Mg, ^{17}O MAS-NMR studies on isotopically enriched materials would be required. Using this approach, Du and Stebbins could unambiguously prove the formation of such non-bridging oxygen species (bound to both, $Si^{(3)}$ and $B^{(2)}$) in a glass of composition $20CaO\text{-}7B_2O_3\text{-}8Al_2O_3\text{-}65SiO_2$.[48]

Table 5: Average isotropic chemical shifts (±0.5 ppm) measured from the center of gravity and *FWHM* values (values in parentheses) as obtained from the ^{29}Si MAS NMR experiments (±0.5 ppm).

Sample	$x = 0$	$x = 5$	$x = 10$	$x = 15$	$x = 20$
$20Na_2O$	-89.0 (14.5)	-92.0 (14.4)	-93.5 (18.0)	-95.4 (19.7)	-96.0 (20.2)
$15Na_2O\text{-}5MgO$	-	-	-	-	-98.0 (21.3)
$10Na_2O\text{-}10MgO$	-92.0 (17.3)	-95.0 (20.9)	-98.6 (17.4)	-101.1 (20.8)	-100.0 (25.2)
$20MgO$	-95.0 (23.5)	-	-	-	-

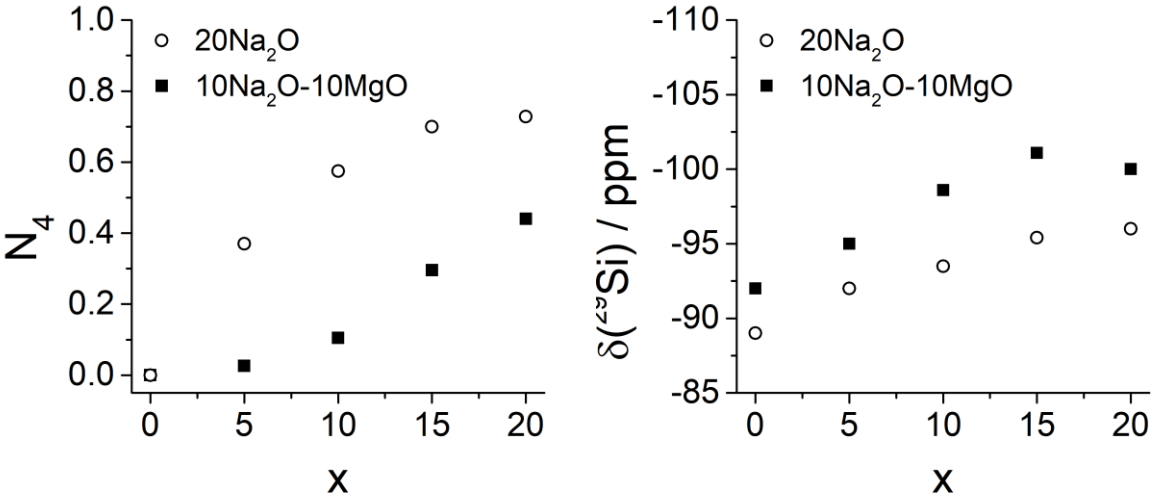

Figure 4: Fraction of four-coordinated boron N_4 (left) and average ^{29}Si chemical shift (measured at center of gravity) (right) vs. the composition in the system $60SiO_2\text{-}(20\text{-}x)Al_2O_3\text{-}xB_2O_3\text{-}20Na_2O$ and $60SiO_2\text{-}(20\text{-}x)Al_2O_3\text{-}xB_2O_3\text{-}10Na_2O\text{-}10MgO$.

^{11}B{^{27}Al} REDOR. The data in Table 1 suggest some synergy of boron and aluminum oxide with regard to the increase of the crack resistance. Evidently, Na-Mg-boroaluminosilicate glasses have higher crack resistance than the analogous individual borosilicate and aluminosilicate glass systems on which they are based. This raises the question whether there are specific preferred boron-aluminum interactions in these glasses, which might result in new structural units that are not realized in their individual constituent glass systems. Such boron-aluminum interactions can be probed, by measuring the strength of the heteronuclear ^{11}B-^{27}Al magnetic dipole-dipole couplings using ^{11}B{^{27}Al} REDOR NMR. As the B$^{(3)}$ and B$^{(4)}$ units can be differentiated spectroscopically, this question can be explored separately for both types of boron species. Figures 5 and S5 summarize the results of these studies, monitoring the B$^{(3)}$ and the B$^{(4)}$ units, respectively. The results illustrate that the B$^{(3)}$ units interact significantly more strongly with Al than the B$^{(4)}$ units do. This latter result agrees with previous findings in sodium aluminoborate glasses, and can be explained based on the concept of a "mutual repulsion" of the anionic Al$^{(4)}$ and B$^{(4)}$ units.[48-50] It may be more useful to think of the residual negative charge on such bridging oxygens (formally, -0.5, as both Al$^{(4)}$ and B$^{(4)}$ have a bond valence of 0.75). This residual charge is higher than for Si$^{(4)}$-O-Al$^{(4)}$ and Al$^{(4)}$-O-B$^{(3)}$ (formally, -0.25) and Si$^{(4)}$-O-Si$^{(4)}$ and Si$^{(4)}$-O-B$^{(3)}$ (zero). These higher anionic charges need more and/or closer modifier cations for charge balance. For large, monovalent cations such as Na^+, it is energetically/volumetrically difficult to bring in enough cations for such charge balance, destabilizing such linkages.

Furthermore, Figure 5 shows the expected result that the strength of the ^{27}Al dipolar field exerted upon the ^{11}B nuclei increases with increasing Al/B ratio in these glasses. Further insights are available based on more quantitative considerations. As previously shown theoretically, in the limit of short evolution times, the normalized REDOR difference signal $\Delta S/S_0$ of the observe-nuclei ^{11}B as a function of the dipolar mixing time NT_R (number of rotor cycles times rotor period) can be analyzed by a parabolic function,[51]

$$\frac{\Delta S}{S_0} = \frac{4}{3\pi^2}(NT_R)^2 f M_{2(\mathrm{B-Al})} \qquad (1)$$

whose curvature is given by the dipolar second moment $M_{2(\mathrm{B\text{-}Al})}$. This quantity can, in turn, be calculated from the B-Al internuclear distance distribution via the van Vleck equation:[52]

$$M_{2(B-Al)} = \frac{4}{15}\left(\frac{\mu_o}{4\pi}\right)^2 I(I+1)\gamma_B^2\gamma_{Al}^2\hbar^2 \sum_{Al} r_{B-Al}^{-6} \qquad (2)$$

In this expression I is the spin quantum number of ^{27}Al, and γ_B and γ_{Al} are the gyromagnetic ratios of the nuclei involved in the dipolar coupling. In expression (1) the calibration factor f accounts for deviations of the experimental value from the theoretical results, based on the specific experimental conditions used. In principle, the above expressions are valid for spin-1/2 nuclei only. If, as in the present case, quadrupolar nuclei are involved the theoretical expressions are more complicated, even though the basic parabolic form persists at short evolution times.[53] In this case, equation (1) still can be used if the calibration factor f is determined by measurements on a crystalline model compound with similar spin dynamics as those measured in the glasses.[54] In the present study the model compound $YAl_3(BO_3)_4$ has been used for this calibration purpose.[55] This model compound presents two three-coordinated boron sites: one of them has six Al-B next nearest neighbors at a distance of 2.99 Å, whereas the other one has two Al-B next nearest neighbor distances of 2.92, 3.04, and 3.74 Å each.[56] From eq. (2) we calculate an average theoretical second moment of 71.80×10^6 rad^2/s^2 for this compound. Analysis of the experimental data via eq. (1) results in an apparent value of $M_{2(\text{B-Al})}$ of 29.9×10^6 rad^2/s^2, leading to a calibration factor of f = 0.416. Applying this factor, we obtain the $M_{2(\text{B-Al})}$ values for the glasses as listed in Table 7. Assuming that the next-nearest neighbor B···Al distances in the glasses are of comparable magnitude as in the model compound, we can use these M_2 values to estimate the mean number of B-O-Al connectivities. Table 6 summarizes the results of this analysis. From these data we conclude that there exists no significant amount of $B^{(4)}$-O-$Al^{(4)}$ connectivities at all in any of these glasses. For the $B^{(3)}$ units, small numbers of Al-O-B connectivities are detectable, which increase with increasing Al/B ratio. Essentially, these numbers are close to those expected from a statistical linking model involving all the network former species $Si^{(4)}$, $B^{(3)}$, $B^{(4)}$, and $Al^{(4)}$. For glasses having the same Al/B ratio there is no significant difference between the values measured for the pure sodium- and for the mixed sodium magnesium containing glasses. Based on these measurements we can conclude that the effect of magnesium does not increase the probability of $Al^{(4)}$-O-$B^{(4)}$ or $Al^{(4)}$-O-$B^{(3)}$ linkages occurring. However, in glasses with the same Al/B ratio, the total number of such linkages does increase because the fraction of four-coordinate boron (which is unconnected to $Al^{(4)}$) is significantly depleted in the Mg-containing glasses.

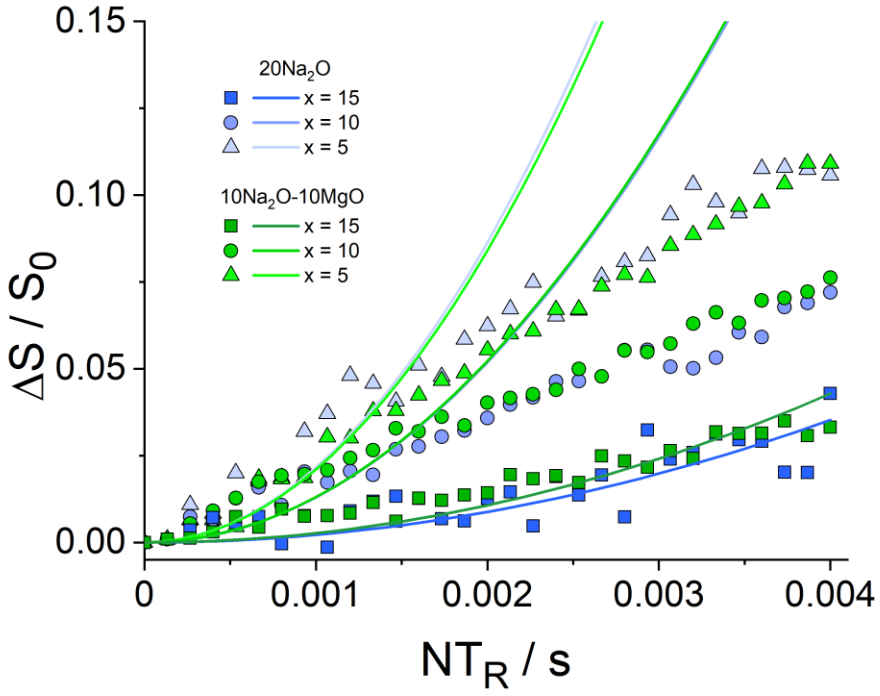

Figure 5: $^{11}B^{(3)}\{^{27}Al\}$ REDOR curves measured for the aluminoborosilicate glasses of the present study. Solid curves are fits to eq. (1)

Table 6: Second moments $M_{2(B\text{-}Al)}$ for the crystalline model compound $YAl_3(BO_3)_4$ and the glassy samples under investigation as derived from REDOR curves' fits. All values have been corrected by a calibration factor of $f = 0.416$, stemming from the ratio of the apparent $M_{2(B\text{-}Al)}$ as experimentally measured for the model compound (29.9×10^6 rad^2/s^2) compared to the theoretical $M_{2(B\text{-}Al)}$ (71.80×10^6 rad^2/s^2) calculated from the crystal structure.

Sample	Species	$M_{2(B\text{-}Al)}$ / $10^6 rad^2 s^{-2}$ (±10%)		$n_{B\text{-}O\text{-}Al}$ (±10%)	
$YAl_3(BO_3)_4$	$B^{(3)}$	71.80		6	
		$20Na_2O$	$10Na_2O$-10MgO	$20Na_2O$	$10Na_2O$-10MgO
$x = 5$	$B^{(3)}$	3.7	4.0	0.31	0.33
	$B^{(4)}$	0.7	-	0.01	-
$x = 10$	$B^{(3)}$	1.9	2.0	0.16	0.17
	$B^{(4)}$	0.3	0.45	0.02	0.04
$x = 15$	$B^{(3)}$	0.45	0.48	0.04	0.03
	$B^{(4)}$	0.2	0.2	0.01	0.01

^{23}Na MAS-NMR: Figure 6 shows the ^{23}Na m = ½ <-> m = -½ central transitions of the studied glasses and the pure boro- and aluminosilicate glasses. Similarly as for ^{27}Al, the asymmetrically broadened lineshapes suggest a high degree of disorder in the local environment around Na. This is supported by the excellent agreement with the one-component Czjzek model deconvolutions. The right-hand side of Figure 6 shows two examples of ^{23}Na TQMAS spectra for samples with x = 10, indicating no further signal components underlying the broad resonance line. From all the TQMAS spectra (see also Figure S6 in the Supporting Information) the isotropic chemical shifts and second order quadrupole effect (*SOQE*) values were determined and stand in good agreement with those determined by the Czjzek deconvolutions. Quadrupole coupling constants and *SOQE* values increase moderately with increasing B content suggesting slightly higher electric field gradients (EFG) at the Na ions interacting with boron rather than with the aluminum species. In both glass series the average isotropic chemical shift values decrease with increasing B content while in the mixed Na-Mg glasses they tend to be lower by several ppm (see Table 7). The interpretation of such subtle chemical shift trends is difficult. In general ^{23}Na chemical shifts reflect both the coordination number and the covalence of the Na-O bonding,[57,58] which, in turn, is affected by the other elements (network formers and modifiers) with which these oxygen atoms are being shared. The shift of the ^{23}Na signals in the mixed Na-Mg glasses towards lower frequencies is also observed in mixed Na-Li borate glasses[58] and indicates that the Na-O bonds are less covalent (and the sites are possibly somewhat expanded) in these glasses than in the corresponding single-alkali glasses.

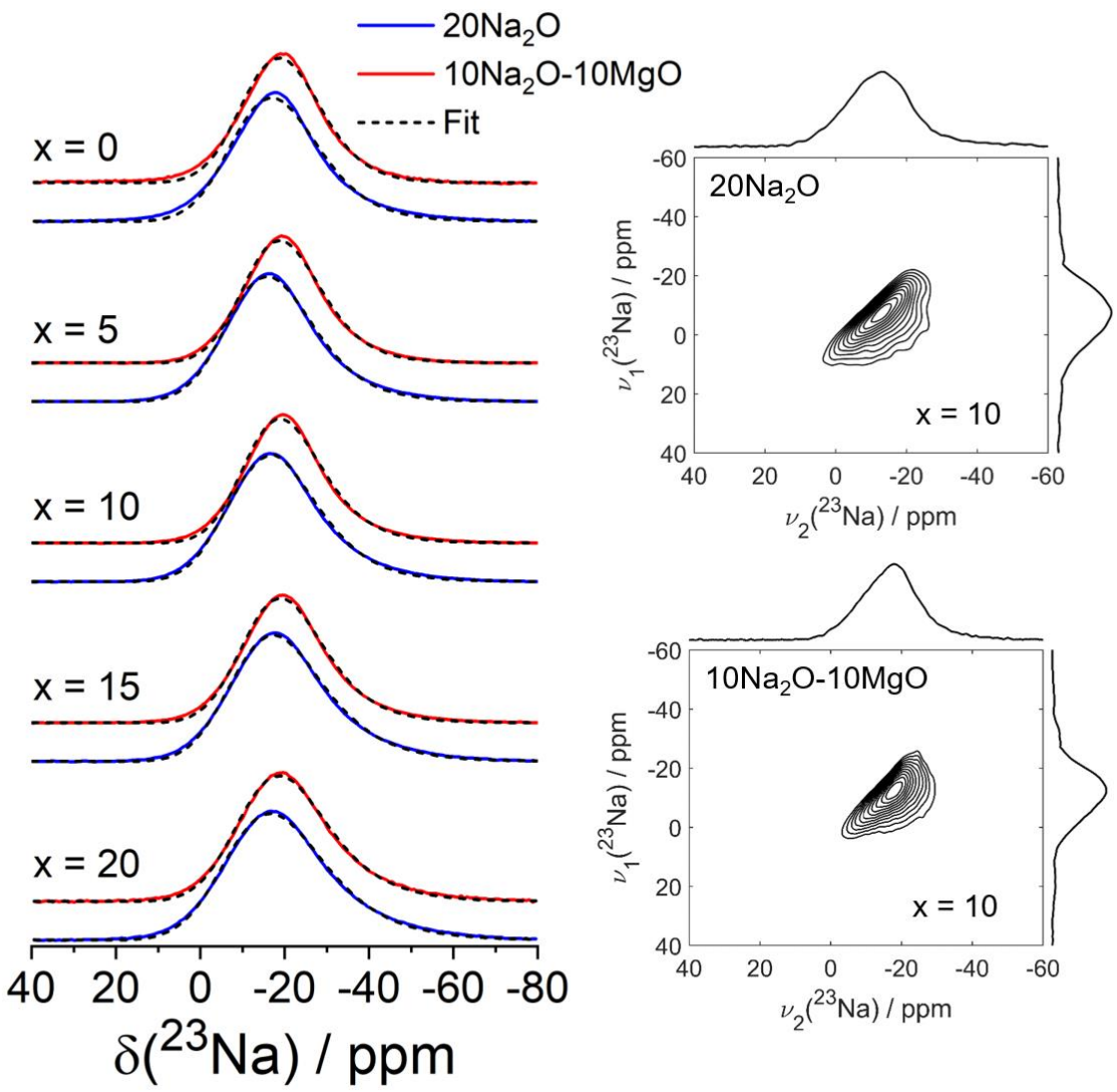

Figure 6: *Left:* ^{23}Na MAS NMR spectra of glasses with compositions $60SiO_2$-(20-*x*)Al_2O_3-*x*B_2O_3 with $20Na_2O$ and $10Na_2O$-10MgO as network modifier. *Right:* Exemplary ^{23}Na TQMAS data of single and mixed modifier glasses with composition *x* = 10.

Table 7: ^{23}Na NMR interaction parameters obtained from MAS NMR analyzed by MAS peak simulation using the Czjzek model and by TQMAS NMR.

Sample	MAS NMR		TQMAS	
	δ_{CS}^{iso} / ppm ± 0.5	C_Q / MHz ± 0.1	δ_{CS}^{iso} / ppm ± 0.2	*SOQE* / MHz ± 0.1
20 Na_2O				
x = 0	-9.4	2.4	-8.9	2.4
x = 5	-8.3	2.4	-7.8	2.4
x = 10	-8.6	2.5	-7.1	2.5
x = 15	-8.5	2.7	-8.3	2.5
x = 20	-7.2	2.8	-6.7	2.6
10 Na_2O-10 MgO				
x = 0	-12.6	2.1	-13.2	2.2
x = 5	-12.3	2.2	-12.5	2.1
x = 10	-12.0	2.3	-12.2	2.4
x = 15	-11.8	2.4	-12.1	2.4
x = 20	-10.4	2.6	-9.8	2.3

^{23}Na static spin echo decay: Figure 7 shows static ^{23}Na spin echo decay measurements on the glasses of this study. The measurements were carried out at low temperatures to eliminate the effect of ionic motion which would cause the resulting second moments to be influenced by dynamically varying dipolar fields and electric field gradients instead of the static local environment. For the samples of this study we have found no further change in the spin echo decay below a temperature of 190 K. A room temperature measurement is reported in Figure S7a of the Supporting Information for comparison, indicating the absolute necessity of measuring these data at sufficiently low temperature. As illustrated in Figure 6 and in its expanded views (Figure S7b), Gaussian behavior is observed within the initial decay region ($0 \leq 2\tau_1 \leq 200$ μs), corresponding to the linear segment of the semi-logarithmic plots of the normalized spin echo intensities $I(2t_1)/I(0)$ versus dipolar mixing time from which the dipolar second moments can be extracted by linear regression using the formula:

$$\ln(I(2\tau_1)/I(0)) = -2\tau_1^2 M_{2(\text{Na-Na})} \qquad (3)$$

corresponding to the established procedure applied previously to such spin echo decay measurements in glasses.[33,54]

At longer dipolar evolution times ($2\tau_1$ > 200 µs), significant deviations from Gaussian behavior are observed, reflecting the influence of higher moments upon the spin echo decay. As the description of the spin echo decay behavior is much more complicated at longer evolution times, this part of the data has not been considered in the analysis.

Figure 7 (bottom right) and Table 8 summarize the results obtained in the present glass system. With the exception of the pure sodium aluminosilicate glass $20Na_2O$-$20Al_2O_3$-$60SiO_2$, the spin echo decay decays in all the other glasses closely resemble each other with second moment values scattering around $2.0\pm0.5\times10^6$ rad^2/s^2. There does not seem to be a compositional dependence on the B/Al ratio in these glasses. The second moment values are similar to those measured in pure sodium borate glasses having comparable cation concentrations.[54] The most remarkable result, however, is the fact that $M_{2(Na\text{-}Na)}$ does not decrease at all, when half of the total Na content is replaced by Mg. The weak compositional dependence in the present system can be understood in terms of the fact that the locus of the sodium ions is correlated with that of the anionic $B^{(4)}$ and $Al^{(4)}$ units to which they are attracted by Coulomb forces. Thus the spatial distribution of the sodium ions mirrors that of the four-coordinate units, which is not necessarily random in space. Therefore, the result of the present study suggests that network former mixing does not occur in the manner of random linkages. In particular $B^{(4)}$-O-$B^{(4)}$, $B^{(4)}$-O-$Al^{(4)}$, and $Al^{(4)}$-O-$Al^{(4)}$ linkages, which would also bring charge-compensating sodium ions into close proximity of each other are being avoided. Only in the boron-free glass $20Na_2O$-$20Al_2O_3$-$60SiO_2$ a significantly larger $M_{2(Na\text{-}Na)}$ value of 7.5×10^6 rad^2/s^2 is measured. This does not necessarily imply the presence of $Al^{(4)}$-O-$Al^{(4)}$ linkages in this glass, however. Rather, the enhanced $M_{2(Na\text{-}Na)}$ value can also be understood to be a consequence of the $Al^{(4)}$-O-$Al^{(4)}$ avoidance. The latter forces the majority of silicon species to have multiple (two to four) Si-O-Al linkages, i.e. tetrahedral configurations of the kind $\{$Al-O-Si-O-Al$\}^{2-}$ which again bring the charge-compensating Na^+ ions into closer proximity. The drastic decrease of $M_{2(Na\text{-}Na)}$ in the glass with composition $10Na_2O$-$10MgO$-$20Al_2O_3$-$60SiO_2$ can then be understood when postulating that such units would preferentially attract the doubly charged Mg^{2+} ions for charge compensation, leading to an effective dispersal of the Na^+ ions.

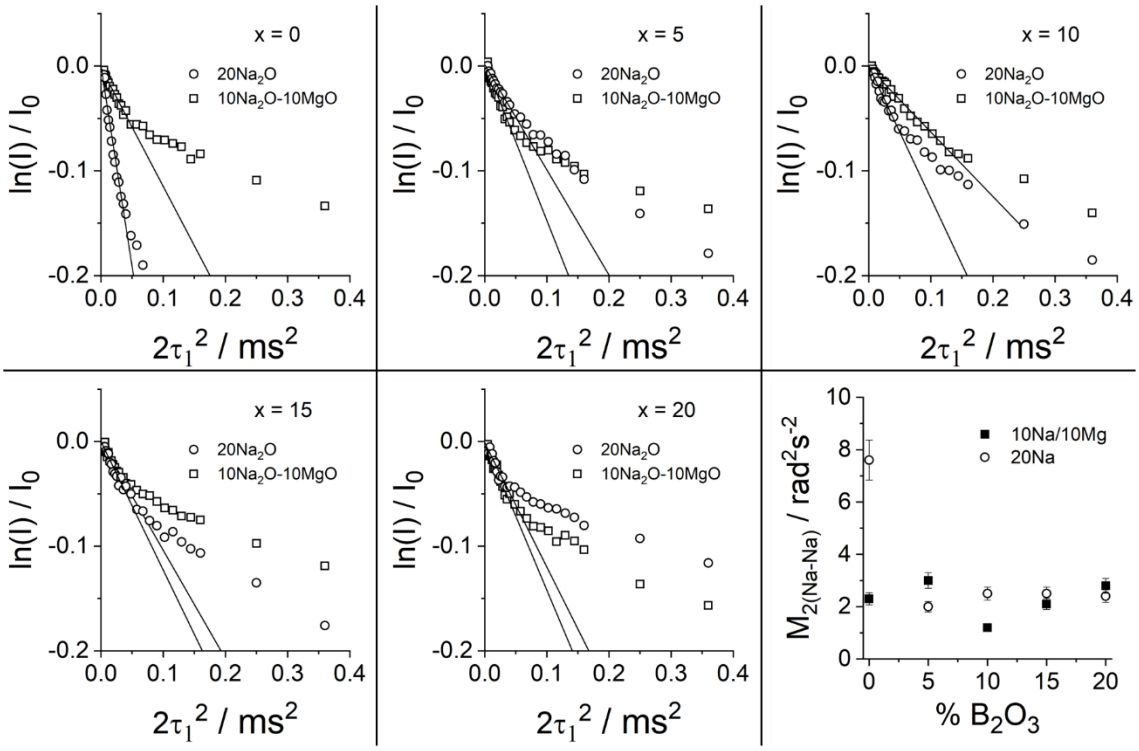

Figure 7: Static ^{23}Na spin echo intensities vs. $2\tau_1^2$ (τ_1 being the interpulse delay in the Hahn spin echo sequence) for the glasses of this study. Solid lines indicate semilogarithmic fits of the data to eq. (3). Bottom right shows an overview of the homonuclear second moments $M_{2(\text{Na-Na})}$, extracted from linear regressions considering data up to $2\tau_1^2 < 0.1$ ms^2. For x = 10 Gaussian behavior was found over a longer delay range for the mixed modifier glass.

^{11}B{^{23}Na} REDOR: In analogy to the above described ^{11}B{^{27}Al} REDOR experiments the measurement of ^{11}B/^{23}Na magnetic dipolar interactions can be investigated individually for both types of boron species present in the glasses. Figure 8 shows the results of ^{11}B{^{23}Na} REDOR measurements on the glasses of this study. Additionally, measurements have been performed under the same conditions for vitreous and crystalline $Na_4B_2O_7$, for calibration purposes, see Table 8.[54] Generally, the REDOR curves of the $B^{(3)}$ and $B^{(4)}$ units closely resemble each other, while the average dipolar interaction strengths between ^{11}B and ^{23}Na are found to be consistently higher for the $B^{(4)}$ species. This is not unexpected because of the anionic character of the $B^{(4)}$ units, resulting in Columbic attraction of the Na^+ ions, which is not the case for the uncharged $B^{(3)}$ units. The second moment values found for the single modifier glasses stay constant within experimental error as the B/Al ratio is varied, suggesting that the local environment of boron with Na^+ ions remains constant in these glasses despite the variation in Na/B ratio from 1:1 in the x =20 glass to 4:1 in the x = 5 glass. The constant $M_{2(\text{B-Na})}$ value for this series of glasses is easily explained in terms of the model based on the preferential attraction of the sodium ions by the $Al^{(4)}$ units. Taking

this effect into consideration the amount of Na^+ available for charge compensating the anionic borate species actually shows little variation across the range of *x*-values. This is also true for the interactions between the sodium ions and the $B^{(3)}$ species. For the latter the $M_{2(B\text{-}Na)}$ values tend to be smaller than for the $B^{(4)}$ species. This result differs from the situation in pure borate glasses, in which the $M_{2(B\text{-}Na)}$ values are identical within experimental error for $B^{(4)}$ and $B^{(3)}$ units.[54] The latter finding is easily explained by the fact that the coordination sphere of the sodium ions is only comprised of the bridging oxygens within the $B^{(3)}$-O-$B^{(4)}$ connectivities. In the present borosilicate glasses the coordination sphere of the sodium ions is comprised of the bridging oxygens within the $B^{(3)}$-O-$B^{(4)}$ and the $Si^{(4)}$-O-$B^{(4)}$ connectivities. The three-coordinate boron species experience a moderately weaker average dipolar field from the ^{23}Na nuclei, as in principle some neutral $B^{(3)}$ units can end up rather remote from sodium ions. On the other hand stronger $^{11}B/^{23}Na$ interactions are expected for that part of the three-coordinate boron inventory made up by $B^{(2)}$ units carrying non-bridging oxygen species (which is, however, likely to be small in the glasses of the present study).

The situation is quite different for the mixed Na-Mg aluminoborosilicate glasses. First of all, the $M_{2(B\text{-}Na)}$ values of the $B^{(4)}$ species are significantly smaller than in the pure sodium-containing glasses, reflecting the decreased Na/B ratios. Secondly, the $M_{2(B\text{-}Na)}$ values decrease significantly as the boron concentration decreases and are thus ***anti-correlated*** with the Na/B ratios. Again this trend can be explained on the basis of a preferred interaction of Na^+ with the $Al^{(4)}$ units, in which case no Na^+ ions would be available to charge compensate the anionic $B^{(4)}$ units in the mixed Na-Mg glasses for x = 5 and 10. Indeed very few $B^{(4)}$ units are formed in these two glasses and the $M_{2(B4\text{-}Na)}$ values found for them are very small. Their numerical values are consistent with the expectation for isolated spin pairs at a Na···B distance of 0.32 pm. Alternatively the values could reflect interactions with multiple ^{23}Na nuclei over longer distance ranges. The compositional dependence of the $M_{2(B3\text{-}Na)}$ values can be discussed analogously.

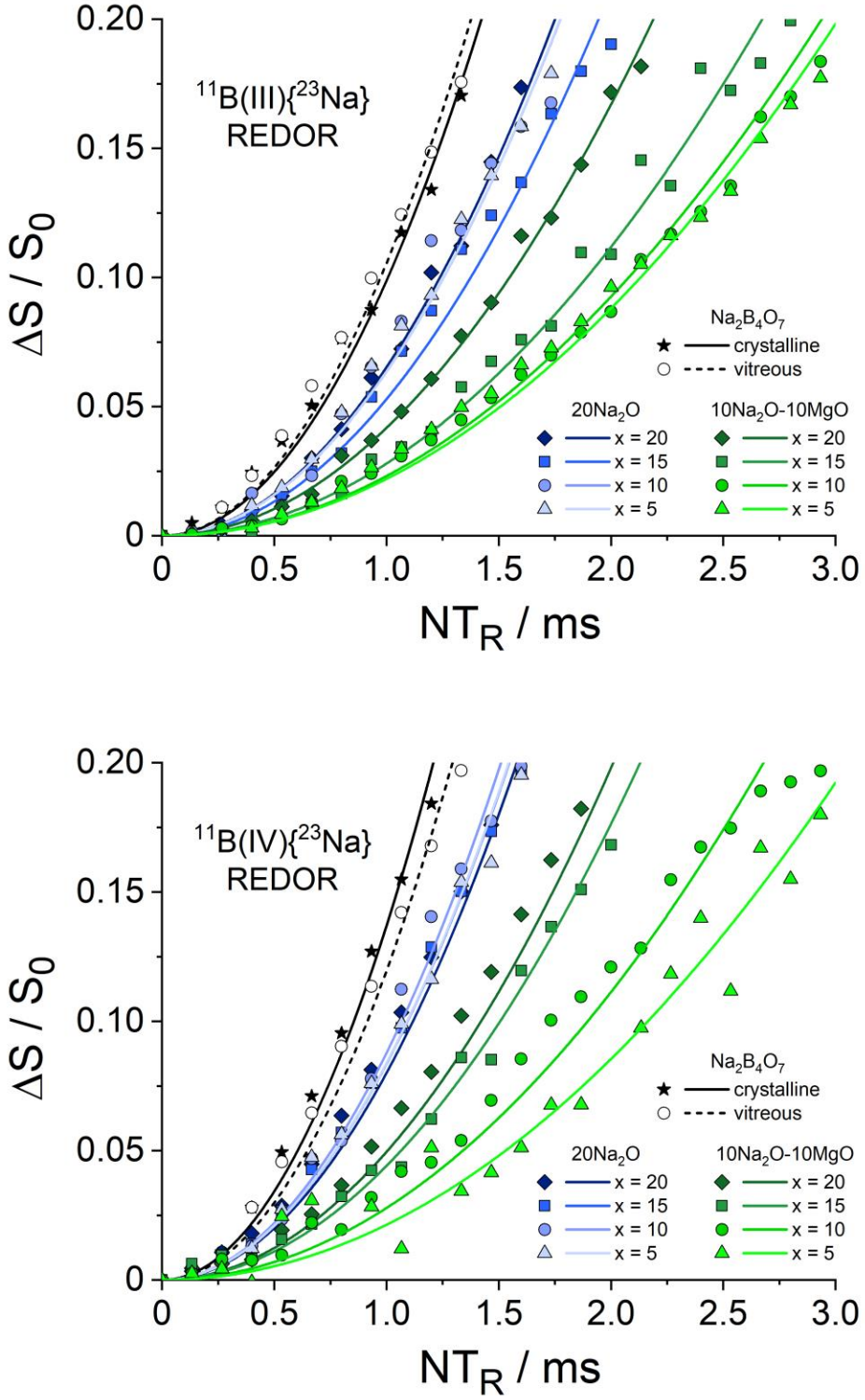

Figure 8: $^{11}B\{^{23}Na\}$ REDOR curves of vitreous and crystalline $Na_2B_4O_7$ and of glasses with compositions $60SiO_2$-$(20\text{-}x)Al_2O_3$-xB_2O_3 with $20Na_2O$ and $10Na_2O$-10MgO as network modifier. *Top:* $B^{(3)}$ observed experiment; *Bottom:* $B^{(4)}$ observed experiment. Solid curves are fits to eq. (1).

Table 8: $M_{2(Na\text{-}Na)}$ and calibrated $M_{2(B\text{-}Na)}$ values (±10%) obtained from $^{11}B\{^{23}Na\}$ REDOR experiments on crystalline and vitreous $Na_2B_4O_7$ and NEG samples. Applied calibration factors were found to be $f = 0.203$ and 0.214 for $B^{(3)}$ and $B^{(4)}$, respectively, based on experiments with $Na_2B_4O_7$ and the crystallographic information available for this compound.[59]

Sample	$M_{2(B(3)\text{-}Na)}$ / 10^6 rad^{2}s^{-2}	$M_{2(B(4)\text{-}Na)}$ / 10^6 rad^{2}s^{-2}	$M_{2(Na\text{-}Na)}$ / 10^6 rad^{2}s^{-2}
$Na_2B_4O_7$			
Vitreous	18.0	23.7	-
Crystalline	19.3	20.7	-
20 Na_2O			
x = 0	-	-	7.6
x = 5	11.6	14.5	2.0
x = 10	11.6	15.2	2.5
x =15	9.6	14.5	2.5
x = 20	11.9	13.8	2.4
10 Na_2O-10 MgO			
x = 0	-	-	2.3
x = 5	4.0	3.7	3.0
x = 10	4.2	4.8	1.2
x =15	5.1	7.6	2.1
x = 20	7.6	8.6	2.8

DISCUSSION

We can now address the compositional changes of the physical properties and the crack resistance as a function of Al/B ratio and evaluate the effect of the substitution of Na_2O by MgO on these properties. For the high-boron glasses (x = 15 and 20) the large fractions of four-coordinated boron contribute to the low molar volumes and high E-modules. For these glasses the increase in molar volume and the decrease in the E-modulus in the mixed cation glasses containing 10 mole% Na_2O and MgO again can be attributed to the significant decrease in N_4 relative to the values in the Na system. For glasses with $x \leq 10$, the influence of the boron coordination upon the physical properties becomes less and less important, however. Here the substitution of Na_2O by MgO

produces a different effect, which is clearly related to the structural organization of the aluminum species and acts in the opposite direction, lowering molar volumes and enhancing E-modulus with increasing Al content and also upon Mg substitution. One possible origin of this enhancement could be a special network former mixing effect arising from preferential Al/B interactions in these glasses. This explanation can be ruled out on the basis of the $^{11}B\{^{27}Al\}$ REDOR data obtained in this study. These data only reveal the suspected mutual repulsion of the anionic four coordinate $Al^{(4)}$ and the $B^{(4)}$ species, which is already well-documented in sodium aluminoborate glasses.[50-52] In contrast, the $B^{(3)}$ units take part in B-O-Al linkages with statistical probability, but their overall concentration is low owing to the low molar fractions of B_2O_3 and alumina. Furthermore, partial substitution of Mg by Na has no influence on the strength of the ^{11}B-^{27}Al magnetic dipole-dipole interactions. On this basis we can certainly discount the possibility that the interaction with Mg stimulates the formation of new structural units characterized by special boron/aluminum next-nearest-neighbor correlations. Nevertheless, because of the $Al^{(4)}$-$B^{(4)}$ avoidance the total number of Al-O-B linkages increases as a consequence of the reduction in N_4, and this may also contribute to the enhanced crack resistance of the Mg-containing glasses as compared to the Mg-free glasses. In contrast to the situation in the pure aluminosilicate endmember glass series, the replacement of Na_2O by MgO does not promote the formation of higher-coordinated ($Al^{(5)}$ and $Al^{(6)}$) species. These species could not be detected by ^{27}Al MAS-NMR within an estimated detection limit of 2%. It is worth pointing out, however, that $Al^{(5)}$ and $Al^{(6)}$) species can be formed in boroaluminosilicate glasses with a CaO/Al_2O_3 ratio of unity, but additional B_2O_3 present.[26]

Overall, the dominant mechanism at work in the present glass series is the control of the overall concentration of four-coordinate structural units by the magnesia component. Four-coordinate units such as $B^{(4)}$ and $Al^{(4)}$ have been previously identified as structural units that are detrimental to the goal of enhanced scratch resistance. The ^{27}Al MAS-NMR spectra reveal that the structure of the present glasses is dominated by the Lewis acid character of the group 13 oxide Al_2O_3, which combines with an equivalent amount of alkaline or alkaline earth oxide to produce charge compensated four-coordinated aluminum species, commonly described as $AlO_{4/2}^-$ (= $Al^{(4)}$) units linked to bridging oxygen. In principle charge compensation of these units can proceed using either Na^+ or Mg^{2+} ions. The analogous structural conversion mechanism can be envisioned in borosilicate glasses. However, the tendency of boron to assume four-coordination is significantly lower than for Al and is highly dependent on glass composition, as discussed in detail by Dell and

Bray.[44] Additional work in the literature has indicated that it also depends on the type of network modifier species.[15-19] As already documented by Kim and Bray, magnesium oxide profoundly decreases the fraction of four-coordinate boron in sodium magnesium borate glasses.[60] In the present glass system, the diminution of N_4 by MgO appears to be similarly dramatic. These results indicate that association of Mg^{2+} with four-coordinate boron is highly disfavored, as is already evident from the impossibility of preparing pure magnesium borosilicate glasses with these network modifier concentrations. If we thus assume that boron cannot be modified by MgO at all to the four-coordinated state, any conversion of $B^{(3)}$ to $B^{(4)}$ units requires an equivalent amount of Na_2O to be available. If, however, Al always takes precedence in its demand for Na^+ species for charge compensating the AlO_4^- units formed, boron modification will be limited by the quantity left over after discounting an amount equivalent to the charge compensation of the aluminate species present. Based on this model we may then come up with a prediction for the concentration of $B^{(4)}$ units. Table 6 summarizes these predicted N_4 values with our experimental data. We find that the experimental N_4 values are consistently lower than those predicted by this idea, indicating a reduced efficiency (about 70%) of this modification process. By making this additional adjustment the fraction of four-coordinated boron can be universally predicted in the present system. The good agreement also confirms the inherent assumption of our model, proposing a strong preference of the AlO_4^- units to be charge compensated by sodium ions rather than by magnesium ions.

The obvious follow-up question then concerns the charge balance and the structural role of the Mg^{2+} ions in this glass system. As previously shown, high-field strength cations tend to promote the formation of non-bridging oxygen species. The NMR data of the present study lend further support to this idea, providing weak evidence for $Si^{(3)}$ units and identifying some highly distorted four-coordinate Al species, which might arise from $Al^{(3)}$ units or $Al^{(4)}$-O-$Al^{(4)}$ linkages. In contrast, the formation of $B^{(2)}$ units appears less likely, based on the ^{11}B NMR lineshapes of the three-coordinate boron species and comparison with literature data on crystalline model compounds with $B^{(2)}$ units.[45] More direct and quantitative evidence on the speciation of non-bridging oxygen could come from ^{17}O MAS-NMR on isotopically labelled glasses.

Alternatively, MgO might not be considered a network modifier, but a network former, producing four- (or even higher-) coordinate Mg in the network, as already proposed by Kim and Bray.[60] In case these magnesium ions are linked to two-coordinate bridging oxygen $MgO_{4/2}^{2-}$ units, the

necessary charge compensation could come from Mg^{2+} ions. It is also possible that both the Mg species and the oxide ions bonded to them have higher coordination numbers, which would result in some clustering.

Table 9: Experimental concentrations of four-coordinated boron and aluminum species, in units of mole% and predicted concentration of $B^{(4)}$ species $[B^{(4)}] = N_4 \times [B]$ based on the model described in the text, assuming boron conversion efficiencies of 100% and 70% (the latter in parentheses), respectively. $[X^{(4)}] = [Al^{(4)}] + [B^{(4)}]$ denotes the overall concentration of four-coordinate species in these glasses.

Sample	$[B^{(4)}]$	$[Al^{(4)}]$	$[X^{(4)}]$	$[B^{(4)}]$calc
20 Na_2O				
x = 0	0	20	20	0
x = 5	1.85	15	16.9	5 (3.5)
x = 10	5.75	10	15.8	10 (7.0)
x =15	10.5	5	15.5	15 (10.5)
x = 20	15.0	0	15.0	20 (14.0)
10 Na_2O-10 MgO				
x = 0	0	20	20	
x = 5	0.13	15	15.1	0
x = 10	1.05	10	11.1	0
x =15	4.44	5	9.4	5(3.5)
x = 20	8.80	0	8.8	10 (7.0)
15 Na_2O-5 MgO				
x = 20	11.0	0	11.0	15 (10.5)
20 MgO				
x = 0	0	17.4	17.4	

CONCLUSIONS

To summarize, the results of the present study suggest that the Mg-driven enhancement of crack resistance in Na-Mg boroaluminosilicate glasses can be related to a reduction in the fraction of four-coordinate boron, producing higher concentrations of non-bridging oxygen species. For

boron-rich glasses (x = 20, 15, 10), this trend is accompanied by the expected decrease in E-modulus. For low-boron glasses, however, the reduction of E-modulus owing to the decrease in N_4 is over-compensated by the strong interaction of the non-bridging oxygen species with the high-field strength cation Mg^{2+}. Finally, in the boron-free aluminosilicate endmember series, the formation of higher-coordinated aluminum contributes to a *simultaneous* increase in both crack resistance and E-modulus. For an advanced understanding of these compositional trends, more structural details regarding the local environment and spatial distribution of the Mg^{2+} ions will be required. Unfortunately, the ^{25}Mg nuclide has very unfavorable NMR detection properties, including a small nuclear magnetic moment, low natural abundance and a large quadrupole moment. While the feasibility of ^{25}Mg NMR in glasses has been demonstrated some time ago,[61-63] applying very high to ultrahigh magnetic field strengths, physical insights into the local environments of magnesium in glasses from the chemical shifts measured have remained somewhat limited. A promising new experimental approach could be the measurement of Mg-selective radial distribution functions based on neutron diffraction experiments with ^{25}Mg enriched glasses. Such work could be combined with NMR studies of the latter, utilizing the toolbox of dipolar spectroscopy, including homonuclear ^{25}Mg spin echo decay and heteronuclear $^{25}Mg/^{11}B$, $^{25}Mg/^{27}Al$ and $^{25}Mg/^{29}Si$ dipolar (REDOR and REAPDOR) spectroscopies. Experiments of this nature are currently under consideration in our laboratories. Ultimately, of course, not only the structure of the annealed glasses is important, but even more important for mechanics are likely the structural rearrangements that occur under stress (indentation). For the elucidation of such structural rearrangements the use of different spectroscopic probes will be required.

ADDITIONAL INFORMATION AVAILABLE

Supporting Materials Section: Description of the REDOR methodology used in the present study, field dependent ^{27}Al MAS-NMR data and Czjzek fits, ^{27}Al SATRAS and TQMAS data, ^{23}Na TQMAS data, $^{11}B\{^{27}Al\}$ REDOR data, fitting details of the ^{23}Na spin echo decays, $^{11}B\{^{23}Na\}$ REDOR data.

AUTHOR INFORMATION

*corresponding author, email: eckerth@uni-muenster.de

There are no conflicting financial interests.

ACKNOWLEDGEMENTS

The NMR equipment used for the measurements was acquired with FAPESP funding, CEPID project 2013-07793-6. We thank Ms. Janete Schultz and Dr. Marcos de Oliveira Jr. for their participation in the initial stages of this work.

REFERENCES

1) Wondraczek, L.; Mauro, J. C.; Eckert, J.; Kühn, U.; Horbach, J.; Deubener, J; Rouxel, T. Towards ultrastrong glasses, *Adv. Mater.* **2011**, *23*, 4578-4586.
2) Sehgal, J. & Ito, S. A new low-brittleness glass in the soda-lime-silica glass family. *J. Am. Ceram. Soc.* **1998**, *81*, 2485–2488.
3) Limbach, R.; Winterstein-Beckmann, A.; Dellith, J.; Möncke, D.; Wondraczek, L. Plasticity, crack initiation, and defect resistance in alkali borosilicate glasses. From normal to anomalous behavior, *J. Non-Cryst. Solids* **2015**, *417-418*, 15-27.
4) Kato, Y.; Yamazaki, H.; Kubo, Y.; Yoshida, S.; Matsuoka, J.; Akai, T. Effect of B_2O_3 content on crack initiation under Vickers indentation test, *J. Ceram. Soc. Jpn.* **2010**, *118*, 792–798.
5) Bechgaard, T. K.; Goel, A.; Youngman, R. E.; Mauro, J. C.; Rzoska, S.J.; Bockowski, M.; Jensen, L. R.; Smedskjaer, M. M., Structure and mechanical properties of compressed sodium aluminosilicate glasses: Role of non-bridging oxygens, *J. Non-Cryst. Solids* **2016**, *441*, 49-57.
6) Rosales-Sosa, G.A.; Masuno, A.; Higo, Y.; Inoue, H. Crack-resistant Al_2O_3-SiO_2 glasses, Scientific Reports, **2016**, *6*, #23620.
7) Januchta, K.; Youngman, R. E.; Goel, A.; Bauchy, M.; Rzoska, S.J.; Bockowsky, M.; Smedskjaer, M. M. Structural origin of high crack resistance in sodium aluminoborate glasses, *J. Non-Cryst. Solids* **2017**, *460*, 54-65.
8) Fredriksen, K. F.; Januchta, K.; Mascaraque, N.; Youngman, R. E.; Bauchy, M.; Rzsoska, S.J.; Bokowsky, M.; Smedskjaer, M. M. Structural compromise between high hardness and crack resistance in aluminoborate glasses, *J. Phys. Chem. B* **2018**, *122*, 6282-6295.
9) Wu, J.; Stebbins, J. F., Quench rate and temperature effects on boron coordination in alminoborosilicate melts, *J. Non-Cryst. Solids* **2010**, *356*, 2097-2108.
10) Wu, J.; Stebbins, J. F. Effects of Cation field strength on the structure of aluminoborosilicate glasses: high-resolution ^{11}B, ^{27}Al, and ^{23}Na MAS-NMR, *J. Non-Cryst. Solids* **2009**, *355*, 556-562.
11) Zhang, X. H.; Yue, Y. L.; Wu, H. T. Effect of cation field strength on structure and properties of boroaluminosilicate glasses, *Mater. Res. Innov.* **2013**, *17*, 212-217.

12) Zhang, X.; Yue, Y.; Wu, H. Effects of MgO/CaO on the structural, thermal and dielectric properties of aluminoborosilicate glasses, *J. Mater. Sci.: Mater. Electron.* **2013**, *24*, 2755-2760.
13) Lee, S. K.; Kim, H. I.; Kim, E. J.; Mun, K. Y.; Ryu, S. Extent of disorder in magnesium aluminosilicate glasses, insights from ^{27}Al and ^{17}O NMR, *J. Phys. Chem*. C **2016**, *120*, 737-749.
14) Morin, E. I.; Stebbins, J. F. Multinucelar NMR investigation of temperature effects on structural reactions involving non-bridging oxygens in multicomponent oxide glasses, *J. Non-Cryst. Solids* **2017**, *471*, 179-186.
15) Morin, E. I.; Wu, J.; Stebbins, J. F. Modifier cation (Ba, Ca, La, Y) field strength effects on aluminum and boron coordination in aluminoborosilicate glasses: the roles of fictive temperature and boron content, *Appl. Phys. A.* **2014**, 116, 479-490.
16) Yamashita, H.; Yoshino, H. Nagata, K.; Inoue, H.; Nakajin, T.; Maekawa, T. Nuclear magnetic resonance studies of of alkaline earth phosphosilicate and aluminoborosilicate glasses, *J. Non-Cryst. Solids* **2000**, *270*, 48-59.
17) Zheng, Q. J.; Youngman, R. J.; Hogue, C: L.; Mauro, J. C.; Potuzak, M.; Smedskjaer, M. M.; Yue, Y. Z. Structure of boroaluminosilicate glasses. Impact of the $[Al_2O_3]/[SiO_2]$ ratio on the structural role of sodium. *Phys. Rev. B* **2012**, *86*, 054203.
18) Backhouse, D. J.; Corkhill, C. L.; Hyatt, N. C.; Hand, R. J. Investigation of the role of Mg and Ca in the structure and durability of aluminoborosilicate glass, *J. Non-Cryst. Solids* **2019**, *512*, 41-52.
19) Jolivet, V.; Josse, L.; Rivoal, M.; Paris, M.; Morizet, Y.; Carole, L, Suzuki-Muresan, T. Quantification of boron in aluminoborosilicate glasses using Raman and ^{11}B NMR, *J. Non-Cryst. Solids* **2019**, *511*, 50-61.
20) Yamashita, H.; Inoue, K.; Nakajin, T.; Inoue, H.; Maekawa, T.; Nuclear magnetic resonance studies of 0.139MO (or M'$_2$O) 0.673SiO_2 (0.188-*x*)Al_2O_3·*x*B_2O_3 (M = Ca, Mg, Ca,Sr, and Ba, M' = Na and K) glasses, *J. Non-Cryst. Solids* **2003**, *331*, 128-136
21) Huang, S.; Li, S.; Wu, F.; Yue, Y. Effect of B_2O_3 on structure and properties of CaO-MgO-B_2O_3-Al_2O_3-SiO_2 glasses, *J. Inorg. Organmet. Polym*. **2015**, *25*, 816-822.
22) Storek W.; Müller, R.; Kunath-Fandrei, G. ^{27}Al and ^{29} Si MAS-NMR investigations of cordierite glass, μ-cordierite, and γ-cordierite, *Solid State Nucl. Magn. Reson.* **1997**, *9*, 227-239.
23) Pierce, E. M.; Reed, L. R.; Shaw, W. J.; Mc. Grail, B. P.; Icenhower, J. P.; Windisch, C.F.; Cordova, E. A.; Broady, J.; Experimental determination of the effect of the ratio of B/Al in glass dissolution along the nepheline ($NaAlSiO_4$-malinkoite ($NaBSiO_4$) join, *Geochim. Cosmochim Acta* **2010**, *74*. 2634-2654.
24) Lee, S. K.; Stebbins, J. F. The degree of aluminum avoidance in aluminosilicate glasses, *Am. Min.* **1999**, *84*, 937-945.
25) Bista, S.; Stebbins. J. F. The role of modifier cations in network cation coordination number increases with pressure in aluminosilicate glasses and melts from 1 to 3 GPa, *Am. Min.* **2017**, *102*, 1657-1666.
26) Bista, S.; Stebbins, J. F.; Wu, J.; Cross, T. J. Structural changes in calcium aluminoborosilicate glasses recovered from pressures of 1.5 to 3 GPa: Interactions of two

network species with coordination number increases, *J. Non-Cryst. Solids* **2017**, *478*, 50-57.

27) Neuville, D. R.; Cormier, L.; Montouillot, V.; Florian, P.; Millot, F.; Rifflet, J. C.; Massiot, D. M. Structure of Mg and Mg/Ca aluminosilicate glasses: ^{27}Al NMR and Raman spectroscopy investigations., *Am. Min*. **2008,** *93*, 1721-1731.
28) Edén, M. ^{27}Al NMR studies of aluminosilicate glasses, Ann. Rep. NMR Spectrosc. **2015**, *86*, 237-331 and references therein.
29) Kato, Y.; Yamazaki, H.; Yoshida, S.; Matsuoka, J.; Kanzaki, M. Measurements of density distribution around Vickers indentation on commercial aluminoborosilicate and soda-lime silicate glasses by using micro Raman spectroscopy, *J. Non-Cryst. Solids* **2012**, *358*, 3473-3480.
30) Sehgal, J.; Ito, S. Brittleness in glass, *J. Non-Cryst. Solids* **1999**, *253*, 126-132.
31) D'Espinose de Lacaillerie, J.B.; Fretigny, C.; Massiot, D. MAS NMR spectra of quadrupolar nuclei in disordered solids: the Czjzek model. *J. Magn. Reson.* **2008**, 192, 244-251.
32) Massiot, D.; Fayon, F.; Capron, M.; King, I.; LeCalvé, S.; Alonso, B.; Durand, J.-O.; Bujoli, B.; Gan, Z.; Hoatson, G. Modelling one and two-dimensional solid-state NMR spectra. *Magn. Reson. Chem.* **2002**, *40*, 70-76.
33) Gee, B.; Eckert, H. ^{23}Na nuclear magnetic resonance spin echo decay spectroscopy of sodium silicate glasses and crystalline model compounds, *Solid State Nucl. Magn. Reson.* **1995**, *5*, 113-122.
34) Medek, A.; Harwood, J. S.; Frydman, L. Multiple-quantum magic-angle spinning NMR: A new method for the study of quadrupolar nuclei in solids. *J. Am. Chem. Soc.* **1995**, *117*, 12779–12787.
35) Gullion, T.; Schaefer, J. Rotational-echo double-resonance NMR. *J. Magn. Reson.* **1989**, *81***,** 196-200.
36) Gullion, T. Measurement of dipolar interactions between spin-12 and quadrupolar nuclei by rotational-echo, adiabatic-passage, double-resonance NMR, *Chem. Phys. Lett.* **1995**, *246*, 325–330.
37) Gullion, T. Measurement of heteronuclear dipolar interactions by rotational-echo, double-resonance nuclear magnetic resonance. *Magn. Reson. Rev* **1997**, *17*, 83-131.
38) Eckert, H. Structural studies of noncrystalline solids using solid state NMR. New experimental approaches and results, *NMR-Basic Principles and Progress* Springer-Verlag, **1994**, *33*, 125-198 and references therein.
39) Eckert, H. Structural characterization of non-crystalline solids and glasses by NMR spectroscopy, *Prog. NMR Spectrosc*. **1992**, *24*, 159-293, and references therein.
40) Deshpande, R. R.; Eckert, H. Sol–gel preparation of mesoporous sodium aluminosilicate glasses: mechanistic and structural investigations by solid state nuclear magnetic resonance, *J. Mater. Chem*. **2009**, *19*, 3419-3426.
41) Jäger, C.; Müller-Warmuth, W.; Mundus, C.; van Wüllen, L. ^{27}Al MAS-NMR spectroscopy of glasses: new facilities by application of 'SATRAS' *J. Non-Cryst. Solids* **1992**, *149*, 209-217.
42) Freude, D.; Haase, J. Quadrupolar effects in solid state nuclear magnetic resonance, J. *NMR Basics Principles and Progress, Special Applications*, Springer Verlag **1993**, *29*, 1-90.

43) Yun, Y. H.; Bray, P. J. Nuclear magnetic resonance studies of the glasses in the system Na_2O-B_2O_3-SiO_2, *J. Non-Cryst. Solids* **1978**, 27, 363-380.
44) Dell, W.; Bray, P. J.; Xiao, S. ^{11}B NMR studies and structural modeling of Na_2O-B_2O_3-SiO_2 glasses of high soda content *J. Non-Cryst. Solids* **1983**, *58*, 1-16.
45) Stebbins, J. F.; Zhao, P.; Kroeker, S. Non-bridging oxygens in borate glasses: characterization by ^{11}B and ^{17}O MAS and 3QMAS NMR, *Solid State Nucl. Magn. Reson.* **2000**, *16*, 9-19.
46) Möncke, D.; Ehrt, D.; Eckert, H.; Mertens, V. Influence of melting and annealing conditions on the structure of borosilicate glasses *Phys. Chem. Glasses* **2003**, *44*, 113-116.
47) Martens, R.; Müller-Warmuth, W. Structural groups and their mixing in borosilicate glasses of various compositions – an NMR study. *J. Non-Cryst. Solids* **2000**, *265*, 167-175.
48) Du, L. S.; Stebbins, J. F. Network connectivity in aluminoborosilicate glasses: A high-resolution ^{11}B, ^{27}Al, and ^{17}O NMR study, *J. Non-Cryst. Solids* **2005**, *352*, 3508-3520.
49) Züchner, L.; Chan, J. C. C.; Müller-Warmuth, W.; Eckert, H. Short and medium range order in sodium aluminoborate glasses: I. Quantification of local environments by high-resolution ^{11}B, ^{23}Na, and ^{27}Al solid state NMR, *J. Phys. Chem., B* **1998,** *102*, 4495-4506.
50) Bertmer, M.; Züchner, L.; Chan, J. C. C.; Eckert, H. Short and medium range order in sodium aluminoborate glasses: II. Site connectivities and cation distributions studied by rotational echo double resonance NMR spectroscopy, *J. Phys. Chem., B* **2000,** *104*, 6541-6553 (2000).
51) Bertmer, M.; Eckert, H. Dephasing of spin echoes by multiple heteronuclear dipolar interactions in rotational echo double resonance NMR experiments. *Solid State Nucl. Magn. Reson.* **1999**, *15*, 139–152.
52) Van Vleck, J. H. The dipolar broadening of magnetic resonance lines in crystals. *Phys. Rev*. **1948**, *74*, 1168-1183.
53) Strojek, W.; Kalwei, M.; Eckert, H. Dipolar NMR strategies for multispin systems involving quadrupolar nuclei: $^{31}P\{^{23}Na\}$ rotational echo double resonance (REDOR) of crystalline sodium phosphates and phosphate glasses. *J. Phys. Chem. B* **2004**, *108*, 7061-7073.
54) Epping, J. D.; Strojek, W.; Eckert, H. Cation environments and spatial distribution in Na_2O-B_2O_3 glasses: New results from solid state NMR, *Phys. Chem. Chem. Phys*. **2005**, *7*, 2384-2389.
55) Deters, H.; de Camargo, A. S. S.; Santos, C. N.; Ferrari, C. R.; Hernandes, A. C.; Ibanez, A.; Rinke, M. T.; Eckert, H. Structural characterization of rare-earth doped yttrium aluminoborate laser glasses using solid state NMR. *J. Phys. Chem. C* **2009**, *113*, 16216–16225.
56) Mészáros, G.; Sváb, E.; Beregi, E.; Watterich, A.; Tóth, M. *Physica B: Condensed Matter* **2000**, 276-278, 310-311
57) Stebbins, J. F. Cation sites in mixed-alkali oxide glasses. Correlations of NMR chemical shift data with site size and distance, *Solid State Ionics* **1998**, *112*, 137-141.
58) Ratai, E.; Chan, J. C. C.; Eckert, H. Local coordination and spatial distribution of cations in mixed-alkali borate glasses, *Phys. Chem. Chem. Phys*. **2002**, *4*, 3198-3208.
59) Krogh Moe, J. The crystal structure of sodium diborate, $Na_2O.2B_2O_3$, *Acta Crystallogr.* B **1974**, *30*, 578-582.
60) Kim, K. S.; Bray, P. J. B^{11} NMR studies of glasses in the system MgO-Na_2O-B_2O_3. *Phys. Chem. Glasses* **1974**, *15*, 47-51.

61) Sen, S.; Maekawa, H.; Papatheodorou, G. N. Short-range structure of invert glasses along the pseudo-binary join $MgSiO_3$-Mg_2SiO_4: Results from ^{29}Si and ^{25}Mg MAS NMR spectroscopy, *J. Phys. Chem. B* **2009**, *113*, 15243-15248.
62) Kroeker, S.; Neuhoff, P. S.; Stebbins, J. F. Enhanced resolution and quantitation from 'ultrahigh' field NMR spectroscopy of glasses, *J. Non-Cryst. Solids* **2001**, *293-295*, 440-445.
63) Shimoda, K.; Nemoto, T.; Saito, K. Local structure of magnesium in silicate glasses: a ^{25}Mg 3QMAS NMR study, *J. Phys. Chem. B* **2008**, *112*, 6747-6752.